THE ANODIZATION OF SILICON IN AN R.F. PLASMA

by

FRANK JOSEPH SCHOLZ

B.Sc., University of Missouri, 1967

A THESIS SUBMITTED IN PARTIAL FULFILMENT OF

THE REQUIREMENTS FOR THE DEGREE OF

MASTER OF APPLIED SCIENCE

in the Department of

Electrical Engineering

We accept this thesis as conforming to the

required standard

Research Supervisor .....

Members of the Committee .....

.....

Head of the Department .....

Members of the Department
of Electrical Engineering
THE UNIVERSITY OF BRITISH COLUMBIA

February, 1971

In presenting this thesis in partial fulfilment of the requirements for an advanced degree at the University of British Columbia, I agree that the Library shall make it freely available for reference and study. I further agree that permission for extensive copying of this thesis for scholarly purposes may be granted by the Head of my Department or by his representatives. It is understood that copying or publication of this thesis for financial gain shall not be allowed without my written permission.

Department of Electrical Engineering

The University of British Columbia
Vancouver 8, Canada

Date March 10, 1970

ABSTRACT

The work contained in this thesis is concerned with the elucidation of the growth mechanism responsible for the formation of silicon dioxide by plasma anodization. Three possible theories for the growth mechanism have been considered; namely, (1) the rate-limiting diffusion theory (2) the classical theory of high-field ionic conduction and (3) the impact ionization theory.

The verification of the applicability of any of the above three theories required the design and construction of (a) an *in situ* film thickness measuring system and (b) a plasma anodization system capable of controlling the substrate temperature.

The experimental data could not be accounted for by either the rate-limiting diffusion or high-field ionic conduction theories, but good agreement was found with predicted results from an impact ionization theory. The development of a suitable impact ionization theory yielded a value for the electron mobility in SiO_2 which was almost identical to the average value calculated from recent Hall effect measurements.

TABLE OF CONTENTS

LIST OF ILLUSTRATIONS

LIST OF TABLES

ACKNOWLEDGEMENT

The author is deeply indebted for the encouragement and guidance received from his research supervisor Dr. D. L. Pulfrey and also for the valuable suggestions and help received from Dr. L. Young.

The author also wishes to thank Mr. G. Olive for many valuable discussions. Grateful acknowledgement is made to senior technician Mr. J. Stuber for the major assistance in the construction of the apparatus and to Mr. J. Lees (Physics Department) for the fabrication of the quartz discharge tube. The author is also grateful for the technical assistance received from Mr. C. G. Chubb, Mr. D. G. Daines and from Mr. H. H. Black for the photographic work.

The author also wishes to thank Miss Linda Morris for typing the manuscript and Mr. S. Graf, Mr. G. Olive and Mr. B. Wilbee for their careful proofreading of the final draft.

The author is grateful for the financial support received from the U. S. Air Force (contract F33615-70-C-1225), and the National Research Council (operating grants 67-7248 and 3392).

I. INTRODUCTION

In silicon integrated device technology it would be desirable to limit the temperature required for the growth of silicon dioxide films. The present commerically used technique of growing silicon dioxide films is by thermal oxidation which requires temperatures in the range of 700 to 1200°C. It would also be desirable to be able to grow silicon dioxide films by a technique that would be compatible with present thin film vacuum technology. A technique which satisfies the above two requirements is plasma anodization which may be described as the growing of an oxide film on a metallic or semiconducting substrate by the application of a positive potential to the substrate when it is immersed in a plasma.

The technique of plasma anodization has been used to grow oxides on many metals and semiconductors e.g. Al, Ta, Mg, Cr, Sb, Bi, Zr, Mn, U, Nb, Ti, Be, Ge, Si and GaAs. Reviews covering the work on plasma anodization up to about the end of 1969 are available[1],[2]. This investigation will be restricted to the plasma anodization of silicon because of the importance of the silicon dioxide film on silicon in integrated device technology.

Utilization of the technique of plasma anodization on silicon was first reported by Nazarova[3]. Ligenza[4] investigated the growth mechanism for anodization in a microwave discharge and reported obtaining a parabolic growth rate that was dependent on the oxygen pressure in the discharge tube. Subsequently Kraitchman[5], using a similar microwave discharge, obtained a growth rate that deviated from a parabolic form by a constant that could be attributed to sputtering of the film occurring simultaneously with its growth. Jorgensen[6] has reported this same

parabolic growth mechanism for field assisted thermal oxidation of silicon. In the investigations of Ligenza and Kraitchman no provisions were made for cooling the silicon sample and temperatures as high as 600°C were believed to have been present. These high temperatures besides negating one of the attractions of the low temperature anodization process also suggest the possibility that field assisted thermal oxidation may have been the operative growth mechanism in these cases also.

The primary aim of this investigation, therefore, is the elucidation of the growth mechanism responsible for the plasma anodization of silicon. Because of the apparent high growth rates in high frequency plasmas, as opposed to d.c. plasmas[1], this investigation was undertaken using a plasma induced by an r.f. generator.

In Chapter II the theories for three growth mechanisms that have been previously considered responsible for the anodization of silicon under various conditions are outlined and modified, where necessary, to fit the conditions of plasma anodization.

Chapter III describes the apparatus used and the experimental procedures followed are outlined in Chapter IV. The experimental results are presented in Chapter V and a discussion of these, in relation to the theories presented in Chapter II, follow in Chapter VI. Chapter VII gives the conclusions which may be drawn from this investigation as well as suggestions for further research.

II. POSSIBLE THEORIES FOR THE ANODIZATION GROWTH MECHANISM

1. Rate-limiting diffusion theory

The rate-limiting diffusion process besides being invoked to explain the microwave plasma anodization of silicon[4],[5] is known to take place during the thermal oxidation of silicon[6],[8]. The theory assumes that some type of oxygen speciesdiffuse across the oxide layer and react with the silicon at the oxide-silicon interface. The growth mechanism may be expressed mathematically as

$$\frac{dD}{dt} = \frac{K}{D} \tag{2.1a}$$

where D is the film thickness, t is time and K is the pressure dependent rate constant. In the work of Kraitchman[5] a sputtering rate constant was introduced into (2.1a), to take account of sputtering of the film occurring simultaneously with its growth, giving

$$\frac{dD}{dt} = \frac{K}{D} - S \tag{2.1b}$$

Kraitchman showed (2.1b) to be applicable for anodization under conditions of constant voltage, constant current and also for the case of no applied potential. (This latter condition is further indication of the possibility of thermal oxidation having taken place.)

By the application of Faraday's Law of electrolysis the ionic current density necessary to produce a growth rate $\frac{dD}{dt}$, for an oxide of formula A_xO_y, is given by

$$j_{ion} = \frac{\rho 2yF}{M} \frac{dD}{dt}, \tag{2.2}$$

where j_{ion} is the ionic current density, ρ is the density of the oxide, M is the molecular weight of the oxide and F is the Faraday (9.65×10^4 coulombs).

By the substitution of (2.1b) into (2.2) one obtains

$j_{ion} = \frac{\rho 2yFK}{M} \cdot \frac{1}{D} - \frac{\rho 2yFS}{M}$ which can be written as

$$j_{ion} = c_1(\frac{1}{D}) - c_2 , \tag{2.3}$$

where c_1 and c_2 are constants.

If the rate-limiting diffusion mechanism describes the film growth in the present investigation, then a plot of j_{ion} vs. 1/D will be a straight line.

2. Classical theory of high-field ionic conduction

For high resistance anodic oxide films (e.g. Ta_2O_5 prepared by solution[9] and d.c. plasma anodization[7] and SiO_2 by solution anodization[10]) the ionic current density flowing through an oxide film due to the application of an electric field can be expressed as[9],[10]

$$j_{ion} = aQ2\alpha n\nu e^{-w/KT} e^{aQ\alpha E/KT} = J_0 e^{BE}, \tag{2.4}$$

where w is the height, with zero applied field, of the periodic potential barrier of half-width α, ν is the vibrating frequency of interstitial ions in the film, n is the mobile ion density, K is Boltzmann's constant, T is the temperature and E is the electric field in the oxide. For a constant voltage, U, applied across the oxide film, of thickness D, the electric field E in the oxide will be U/D so that (2.4) becomes

$$j_{ion} = J_0 e^{BU/D}. \tag{2.5}$$

Taking the common logarithm of (2.5) gives

$$\log_{10}(j_{ion}) = \log_{10}(J_0) + \frac{BU}{D} \log_{10} e. \tag{2.6}$$

A plot of $\log_{10}(j_{ion})$ vs. 1/D will be a straight line provided that U and T remain constant.

3. Impact ionization theory

This theory was put forward by Fritzsche[11],[12] to explain his data obtained in the solution anodization of silicon.

The basic assumption of the theory is that every ionizing collision produces one extra free electron and one mobile ion. This suggests that the film may grow by cation migration, the cations being silicon ions.

Fritzshe has derived an equation (6.3) relating total current density to the inverse of the time, the latter being measured from the instant of application of constant voltage. This equation is based on the assumptions that the film grows little, relative to the initial film thickness, after constant voltage is applied and that the film thickness is equivalent to many electron mean-free paths. These assumptions, as will be shown in Chapter VI, are not applicable to the plasma anodization results presented in this thesis. Thus in this section modifications of the impact ionization theory have been made to make it relevant to r.f. plasma anodization.

The impact ionization theory can be developed in the following way. Figure 2.1 shows the silicon-silicon dioxide interface and the silicon dioxide-plasma interface.

n_o ≡ the concentration of electrons excited thermally in the SiO_2 film

n_{inj} ≡ the concentration of electrons injected into the SiO_2 film from the plasma

n_{coll} ≡ the concentration of mobile ions produced by collision in the SiO_2 film

Q ≡ absolute value of an electronic charge

a ≡ the number of electronic charges carried by a cation

μ_{el} ≡ the mobility of electrons in the SiO_2 film

μ_{ion} ≡ the mobility of ions in the SiO_2 film

E ≡ the electric field in the oxide film

D ≡ the oxide film thickness

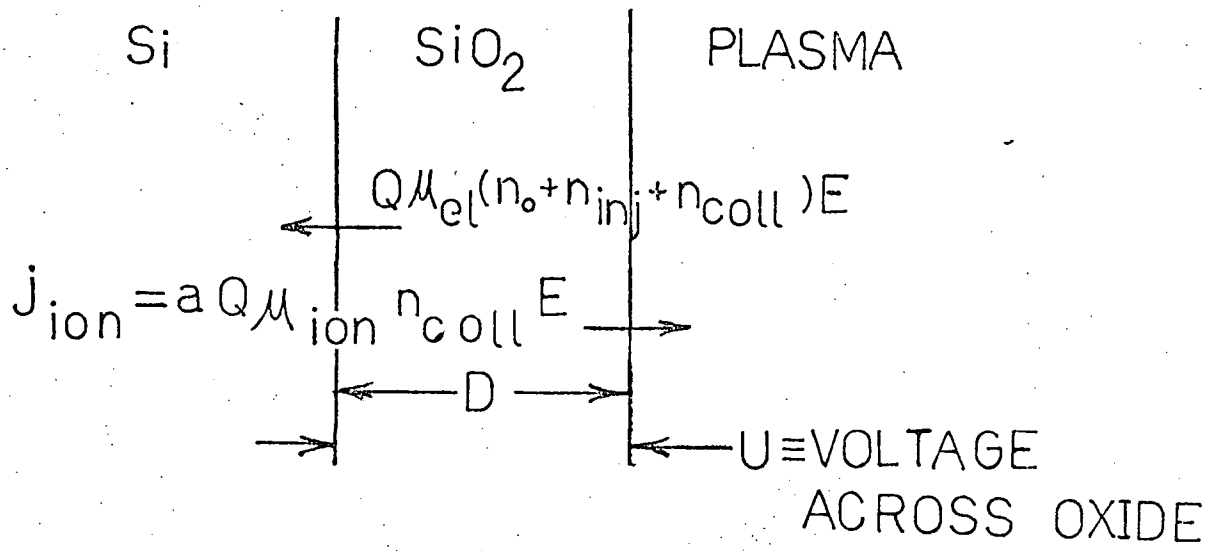

Fig. 2.1

Due to impact ionization there will be a postive ion current density toward the oxide surface given by

$$j_{ion} = aQ\mu_{ion}n_{coll}E. \tag{2.7}$$

There will also be an electron current density at the SiO_2 - Si interface given by

$$j_{el} = Q\mu_{el}(n_o + n_{inj} + n_{coll})E. \tag{2.8}$$

The total current density measured in the external circuit will be given by the sum of j_{ion} and j_{el} or

$$j_{total} = Q\mu_{el}(n_o + n_{inj} + n_{coll})E + aQ\mu_{ion}n_{coll}E. \tag{2.9}$$

The ionic current efficiency, η, is thus defined by

$$\eta = \frac{j_{ion}}{j_{total}} = \frac{aQ\mu_{ion}n_{coll}E}{Q\mu_{el}(n_o + n_{inj} + n_{coll})E + aQ\mu_{ion}n_{coll}E}.$$

Defining the mobility ratio by $q \equiv \frac{\mu_{el}}{\mu_{ion}}$, and the leakage current density by

$$j_{leak} \equiv Q\mu_{el}(n_o + n_{inj})E^{*}. \tag{2.10}$$

The ionic current efficiency can thus be written as

$$\eta = \frac{j_{ion}}{j_{leak} + j_{ion}(1 + \frac{q}{a})} \tag{2.11}$$

Hence the ionic current density can be expressed as

$$j_{ion} = \frac{j_{total} - j_{leak}}{(1 + \frac{q}{a})} \tag{2.12}$$

and η can be expressed as

$$\eta = \frac{1}{(1 + \frac{q}{a})} - \frac{j_{leak}}{(1 + \frac{q}{a})} \cdot \frac{1}{j_{total}}. \tag{2.13}$$

---

* This is not the usual definition of leakage current, but is the total current density that would result if no ionization collisions took place.

The next step in developing the theory is to find a relationship between n_{coll} and the film thickness. The time for an electron to obtain ionization energy while being accelerated in the oxide film is denoted by t_i and the average velocity of an electron through the oxide film is denoted by v. The distance an electron will travel in time t_i is vt_i and the expression for n_{coll} can be shown to be

$$n_{coll} = (n_o + n_{inj})(\tfrac{1}{2}2^{D/vt_i} - 1). \tag{2.14}$$

t_i can be expressed[13] as

$$t_i = t_I e^{t_I/\tau},$$

where t_I is the time required for an electron to acquire an energy QI under free acceleration and τ is the mean time between collisions of all types in the SiO_2 film. The electron free acceleration time t_I can be expressed in terms of the ionization potential, I, and the electronic mass, m, by

$$t_I = \frac{\sqrt{2IQm}}{QE} .$$

Fritzsche has not expressed the average electron velocity, v, in terms of the electric field and he has also assumed that vt_i can be taken as constant during constant voltage anodization. In this thesis the average electron velocity will be taken as

$$v = \mu_{el}E . \tag{2.15}$$

Thus vt_i is written as

$$vt_i = \frac{\mu_{el}\sqrt{2IQm}}{Q} e^{\sqrt{2IQm}/\tau QE}$$

or for a constant voltage U applied across the oxide film vt_i can be expressed as

$$vt_i = \frac{\mu_{el}\sqrt{2IQm}}{Q} e^{\frac{\sqrt{2IQm}}{\tau UQ} D} \quad . \tag{2.16}$$

Using (2.7), (2.10), (2.14), (2.16) and the definition of q the ionic current density can be expressed as a function of D for a constant voltage U as

$$j_{ion} = \frac{j_{leak}}{(\frac{q}{a})} \left[\frac{1}{2}^{\left[\frac{QD}{\mu_{el}\sqrt{2IQm}} e^{\frac{-\sqrt{2IQm}}{\tau UQ} D}\right]} - 1 \right] \tag{2.17}$$

Fritzsche[12] has suggested that j_{leak} and q will remain constant over a sizeable range of values of j_{total}. If we follow this assumption then the values of j_{leak} and $(\frac{q}{a})$ can be calculated from an experimental plot of ηvs. j_{total} by taking two points $(j_{total\ 1}, \eta_1)$ and $(j_{total\ 2}, \eta_2)$ and substituting these points into (2.13) and solving these two simultaneous equations for j_{leak} and $(\frac{q}{a})$ giving

$$j_{leak} = \frac{(\eta_1 - \eta_2) j_{total\ 1} j_{total\ 2}}{\eta_1 j_{total\ 1} - \eta_2 j_{total\ 2}} \tag{2.18}$$

and

$$\frac{q}{a} = \frac{j_{total\ 1} - j_{total\ 2}}{\eta_1 j_{total\ 1} - \eta_2 j_{total\ 2}} - 1 \quad . \tag{2.19}$$

In order to use (2.17) it will be necessary to obtain values of μ_{el} and τU which can be calculated as follows. Using (2.7), (2.10), (2.14) and the definition of q one can obtain the expression

$$2 \cdot \left[\frac{j_{ion}}{(\frac{j_{leak}}{\frac{q}{a}})} + 1 \right] = 2^{D/vt_i} \quad . \tag{2.20}$$

By taking two points on the experimental curve of j_{ion} vs. D i.e. $(D_1, j_{ion\ 1})$

and $(D_2, j_{ion\ 2})$ one can calculate two other sets of points of D and vt_i $(D_1, vt_{i\ 1})$ and $(D_2, vt_{i\ 2})$ using (2.20). The two sets of points of D and vt_i can be substituted into (2.16) giving two equations which can be solved for μ_{el} and τU giving

$$\mu_{el} = \frac{(vt_i)_1 Q}{\sqrt{2IQm}} \; e^{\frac{-D_1}{D_1-D_2}} \ln\left[\frac{(vt_i)_1}{(vt_i)_2}\right] \tag{2.21}$$

and

$$\tau U = \frac{\sqrt{2IQm}\,(D_1-D_2)}{Q \ln\left[\frac{(vt_i)_1}{(vt_i)_2}\right]} \; . \tag{2.22}$$

Note that it is not necessary to know the value of U in order to calculate μ_{el} and τU, though the value of τ cannot be determined independently of U. Substituting μ_{el} and τU into (2.17) gives

$$j_{ion} = \frac{j_{leak}}{\left(\frac{q}{a}\right)} \left[\frac{1}{2} 2^{\left\{\frac{D}{(vt_i)_1} e^{\frac{D_1-D}{D_1-D_2} \ln\left[\frac{(vt_i)_1}{(vt_i)_2}\right]}\right\}} - 1 \right], \tag{2.23}$$

which can be used to draw a graph of j_{ion} vs. D in order to see if the impact ionization theory agrees with the experimental plot of j_{ion} vs. D.

Two features of (2.17) should be noted. First the ionic current density will be zero when

$$De^{\frac{-\sqrt{2IQm}}{\tau U} D} = \frac{\mu_{el}\sqrt{2IQm}}{Q} \; . \tag{2.24}$$

Equation (2.24) can be solved graphically, as shown in Fig. (2.2), giving the limiting oxide film thickness, D_{max}, and the minimum oxide thickness, D_{min}, for which impact ionization can take place for a given

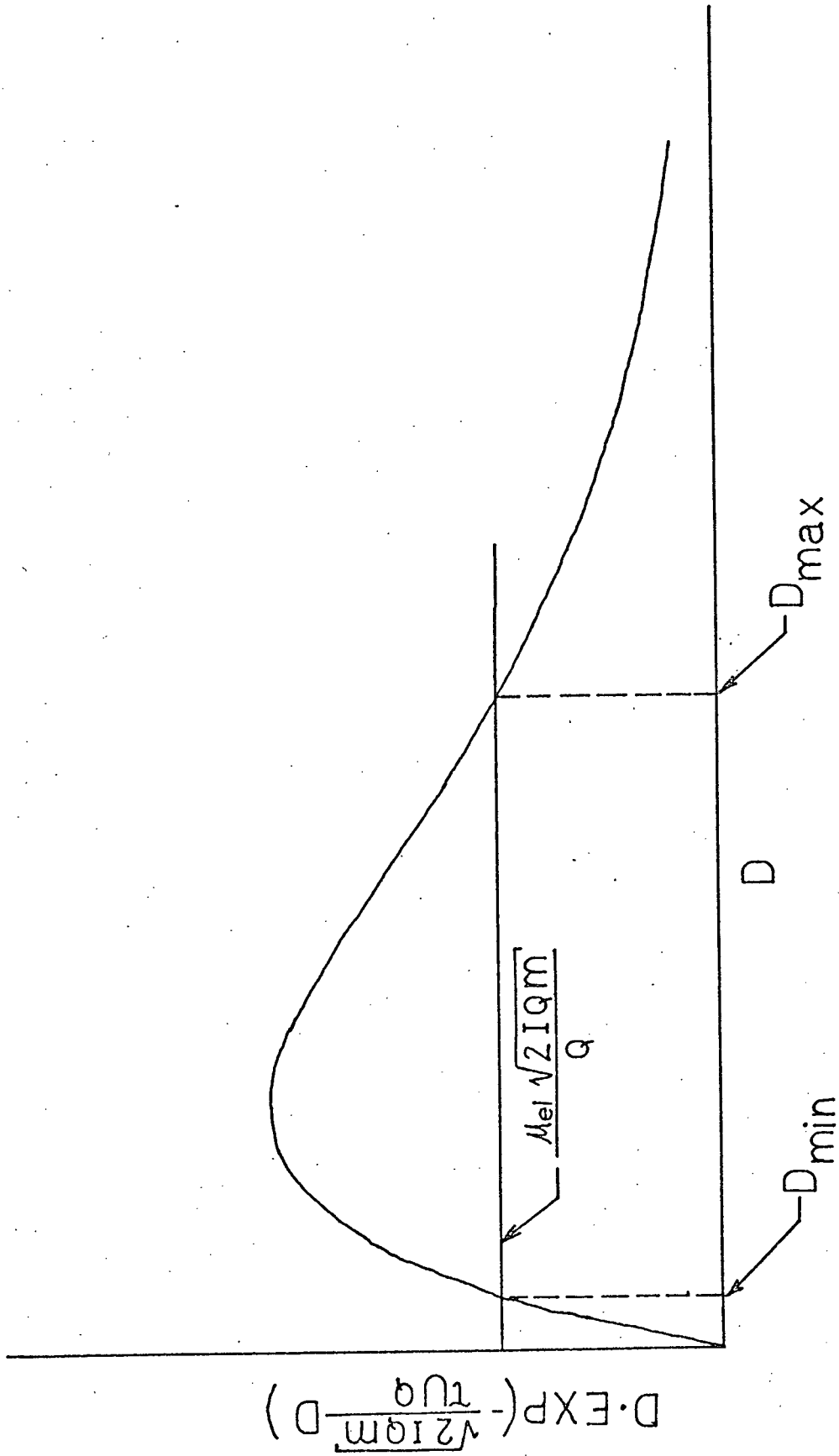
$D \cdot EXP(-\frac{\sqrt{2 I Q m}}{\tau U_Q} D)$
$\frac{\mu_{el} \sqrt{2 I Q m}}{Q}$
D_{min}
D_{max}
D

Fig. 2.2

constant value of voltage. It will be shown that U will not be completely constant, for a constant voltage applied to the sample, and may increase by about 21% of its initial value, for the range of current considered in this investigation, resulting in a higher value of D_{max} than would be predicted for a constant voltage.

For the second feature of (2.17) it is necessary to take the derivative of j_{ion} with respect to D. To simplify the expression for the derivative let $A = \frac{\sqrt{2IQm}}{Q}$ so that the derivative becomes

$$\frac{dj_{ion}}{dD} = \frac{1}{(\frac{q}{a})} \frac{dj_{leak}}{dD}\left[\frac{1}{2}2\left[\frac{D}{\mu_{el}A} e^{\frac{-AD}{\tau U}}\right] - 1\right] + \frac{j_{leak}\ln 2}{2(\frac{q}{a})}2\left[\frac{D}{\mu_{el}A} e^{\frac{-AD}{\tau U}}\right]\frac{-AD}{e^{\tau U}}\frac{}{\mu_{el}}\left[\frac{1}{A} - \frac{D}{\tau U}\right]. \tag{2.25}$$

This derivative was taken with U assumed to be constant which may, as pointed out above, not be completely true in practice. If j_{leak} is constant with D then $\frac{dj_{leak}}{dD} = 0$ and (2.25) becomes

$$\frac{dj_{ion}}{dD} = \frac{j_{leak}\ln 2}{2(\frac{q}{a})\mu_{el}}2\left[\frac{D}{\mu_{el}A} e^{\frac{-AD}{\tau U}}\right]\frac{-AD}{e^{\tau U}}\left[\frac{1}{A} - \frac{D}{\tau U}\right].$$

$\frac{dj_{ion}}{dD}$ has a value of zero when $D = \frac{\tau U}{A}$ (i.e. $\tau = t_I$). This is equivalent to saying that the maximum ionic current density is obtained when the time between collisions is equal to the time required for an electron to acquire an energy QI under free acceleration which would be the condition for the most efficient impact ionization.

Let us consider the situation of a constant total current density applied to the sample. The total current density may be written as

$$j_{total} = j_{leak} + (1 + \frac{q}{a}) j_{ion} .$$

By using (2.17) with $\frac{U}{D} = E$ the total current density can be written as

$$j_{total} = Q\mu_{el}(n_0 + n_{inj})E\left[1 + (\frac{a}{q} + 1)(\frac{1}{2}2^{\left[\frac{QD}{\mu_{el}\sqrt{2IQm}} e^{\frac{-\sqrt{2IQm}}{\tau QE}}\right]} - 1)\right] . \qquad (2.26)$$

For a constant total current density (2.26) must be constant. Inspection of (2.26) shows that the condition of a constant current density cannot be attained by keeping the field constant across the oxide film for as the film grows D will increase and the total current density would increase even if E were kept constant. The variation of $(n_0 + n_{inj})$ with D is also an unknown factor which must be considered.

4. Summary

The three anodization theories considered in this chapter can be distinguished by the predicted dependencies of j_{ion} on D or 1/D. To test whether the rate-limiting diffusion theory is applicable it does not matter if constant current or constant voltage anodization is used, whereas the high-field ionic conduction theory and the impact ionization theory are analyzed more easily under conditions of constant voltage anodization. Thus constant voltage anodization has been used in this investigation. In addition attempts have been made to keep the substrate temperature and the discharge pressure constant during oxide film growth.

III APPARATUS

1. The in situ film thickness measuring system

For all of the three theories listed in Chapter II a knowledge of the dependence of film thickness on time is required.

A simple method of obtaining film thickness data is through optical reflectivity measurements[21].

The power reflection coefficient, R_{power}, for light incident at an angle ϕ_o from the normal to a non-absorbing film of thickness D located on a substrate is given by

$$R_{power} = R_{total} R^*_{total}, \tag{3.1}$$

where R_{total} is the total amplitude reflection coefficient for the electric filed vector and is given by[14]

$$R_{total} = \frac{r_1 + r_2 e^{-2i\delta}}{1 + r_1 r_2 e^{-2i\delta}} . \tag{3.2}$$

The Fresnel amplitude reflection coefficient at the air-film interface is denoted by r_1 and the Fresnel coefficient at the film-substrate interface is denoted by r_2. The change in phase of the light on traversing the film is denoted by δ and is given by $\delta = \frac{2\pi}{\lambda} n_1 D \cos\phi_1$, where λ is the wavelength of the light used, n_1 is the refractive index of the film, D is the film thickness, and ϕ_1 is the angle of refraction of the light in the film given by Snell's Law as $\sin\phi_o = n_1 \sin\phi_1$.

Equations (3.1) and (3.2) form the basis for the method of film thickness measurement used in this investigation.

Figure 3.1 shows the arrangement of the optical film thickness measuring system. By following the signals through the apparatus shown in Fig. 3.1 it can be seen that the input voltage pulse amplitude to

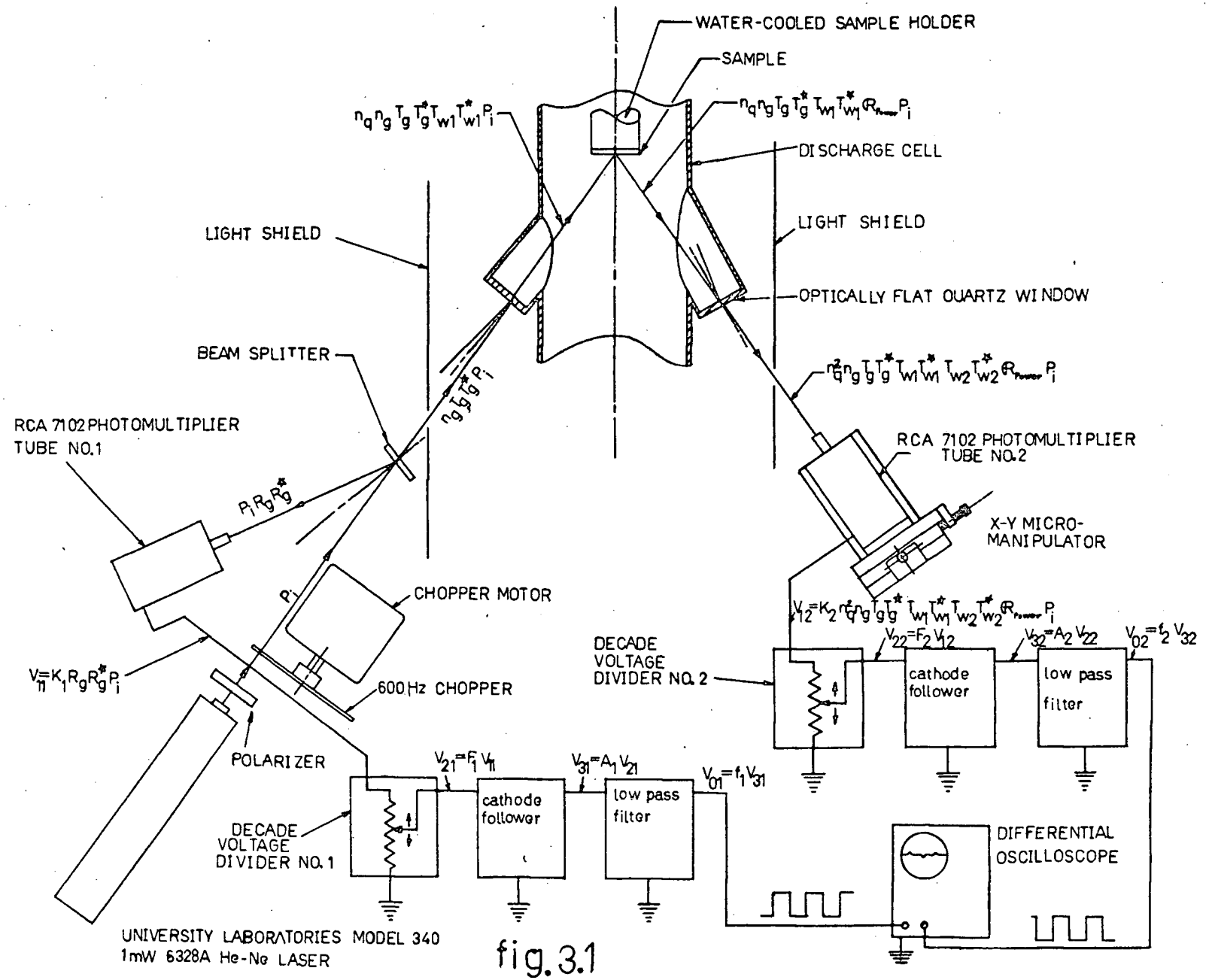
WATER-COOLED SAMPLE HOLDER
SAMPLE
DISCHARGE CELL
LIGHT SHIELD
LIGHT SHIELD
OPTICALLY FLAT QUARTZ WINDOW
BEAM SPLITTER
RCA 7102 PHOTOMULTIPLIER TUBE NO.1
RCA 7102 PHOTOMULTIPLIER TUBE NO.2
X-Y MICRO-MANIPULATOR
CHOPPER MOTOR
600 Hz CHOPPER
POLARIZER
DECADE VOLTAGE DIVIDER NO. 2
cathode follower
low pass filter
DECADE VOLTAGE DIVIDER NO. 1
cathode follower
low pass filter
DIFFERENTIAL OSCILLOSCOPE
UNIVERSITY LABORATORIES MODEL 340
1mW 6328A He-Ne LASER

fig. 3.1

oscilloscope input #2 is

$$v_{02} = f_2 A_2 F_2 K_2 n_q^2 n_g T_g T_g^* T_{w1} T_{w1}^* T_{w2} T_{w2}^* R_{power} P_i \tag{3.3}$$

and the input voltage pulse amplitude to oscilloscope input #1 is

$$v_{01} = f_1 A_1 F_1 K_1 P_i R_g R_g^*. \tag{3.4}$$

R_g denotes the amplitude reflection coefficient of the beam splitter and the T's are amplitude transmission coefficients with the subscripts referring to:- g, the beam splitter, w1 the entry window and w2 the exit window. n_g is the refractive index of the beam splitter, n_q is the refractive index of the quartz windows, F_1 and F_2 are the readings for voltage dividers #1 and #2 respectively, K_1 and K_2 are the proportionality constants of photomultipliers #1 and #2, respectively, A_1 and A_2 are the gains of the two cathode followers and f_1 and f_2 are the factors by which the amplitudes of the rectangular pulses are attenuated in passing through the low pass filter.

By adjusting voltage divider #2 such that $v_{01} = v_{02}$, which gives a zero output on the oscilloscope, one obtains

$$\frac{F_1}{F_2} = \frac{f_2 A_2 K_2 n_q^2 n_g T_g T_g^* T_{w1} T_{w1}^* T_{w2} T_{w2}^*}{f_1 A_1 K R_g R_g^*} R_{power}. \tag{3.5}$$

By taking the logarithm of (3.5) one obtains

$$\log_{10}\left(\frac{F_1}{F_2}\right) = \log_{10}\left(\frac{f_2 A_2 K_2 n_q^2 n_g T_g T_g^* T_{w1} T_{w1}^* T_{w2} T_{w2}^*}{f_1 A_1 K_1 R_g R_g^*}\right) + \log_{10}(R_{power}). \tag{3.6}$$

The first term on the right hand side of (3.6) is a constant of the optical system so that (3.6) may be written as

$$\log\left(\frac{F_1}{F_2}\right) - (\text{constant of system}) = \log_{10}(R_{power}). \tag{3.7}$$

The right hand side of (3.7), $\log_{10}(R_{power})$, can be plotted against D, the film thickness, for a measured angle ϕ_o and for different values of n_1. For a non-absorbing film n_1 will be real and $\log_{10}(R_{power})$ will be a periodic function of D having maxima and minima as shown in Fig. 3.2. The value of n_1 may be obtained by taking the difference between the maxima and minima values of $\log_{10}(\frac{F_1}{F_2})$, defined by

$$\Delta\log_{10}(\frac{F_1}{F_2}) \equiv [\log_{10}(\frac{F_1}{F_2})]_{max} - [\log_{10}(\frac{F_1}{F_2})]_{min},$$

and then determining what value of n_1 will give a plot of $\log_{10}(R_{power})$ vs. D with a difference between its maxima and minima, defined by

$$\Delta\log_{10}(R_{power}) \equiv [\log_{10}(R_{power})]_{max} - [\log_{10}(R_{power})]_{min},$$

such that

$$\Delta\log_{10}(\frac{F_1}{F_2}) = \Delta\log_{10}(R_{power}).$$

The value of the optical system constant can be determined by taking the average value of the differences between the maxima of $\log_{10}(\frac{F_1}{F_2})$ and the maxima of $\log_{10}(R_{power})$ or the minima of $\log_{10}(\frac{F_1}{F_2})$ and the minima of $\log_{10}(R_{power})$ or the average value of both differences so that

$$\text{(constant of the system)} = [\log_{10}(\frac{F_1}{F_2})]_{max} - [\log_{10}(R_{power})]_{max} =$$

$$[\log_{10}(\frac{F_1}{F_2})]_{min} - [\log_{10}(R_{power})]_{min}, \qquad (3.8)$$

where the value of n_1 in the equation of $\log_{10}(R_{power})$ was determined from the procedure explained above.

The film thickness vs. time curve can be obtained by the following procedure: one first subtracts the system constant from each

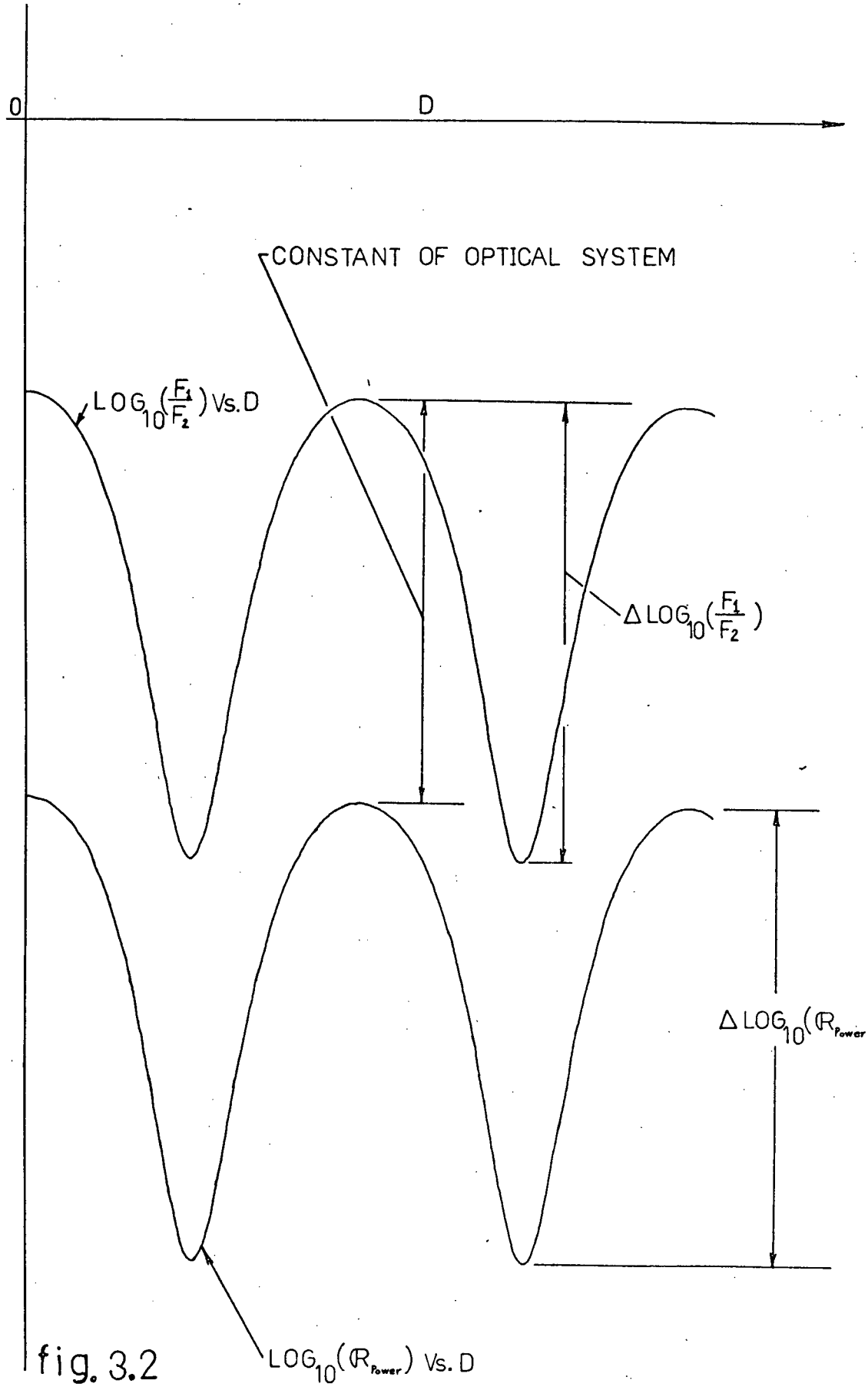
0
D
CONSTANT OF OPTICAL SYSTEM
LOG10(F1/F2) Vs.D
ΔLOG10(F1/F2)
ΔLOG10(RPower)
LOG10(RPower) Vs. D

fig. 3.2

measured value of $\log_{10}(\frac{F_1}{F_2})$ and determines what film thickness would make $\log_{10}(R_{power})$ have the same value, that is what value of D will satisfy (3.7).

There are many values of D that will satisfy (3.7), but there is little chance of ambiguity in determining the correct value of D if one starts growing the film from a known initial film thickness and also consults an interference colour-thickness table[17]. After having determined the correct value of D for each value of $\log_{10}(\frac{F_1}{F_2})$-(constant of system) and having recorded the time at which each measurement of $\log_{10}(\frac{F_1}{F_2})$ was made then one has available the necessary points for plotting a curve of D vs. time.

In the practical thickness measuring system extensive electrical and optical shielding was necessary in order to permit measurement with the plasma on. The photomultipliers were screened from most of the plasma by aluminium sheet metal painted matt black and narrow band optical filters, centered at the laser frequency, were used on each photomultiplier and the light was allowed to reach them only after traveling down 2" long, 1/4" i.d. copper tubes that had been painted matt black. Electrical interference from the r.f. generator, being received by the differential oscilloscope, was eliminated by the installation of 6-element Butterworth low pass filters. Cathode follower circuitry was used to prevent loading of the decade voltage divider boxes by the filters.

A detailed analysis of the percentage error involved in this method of thickness measurement is difficult to carry out, but some of the possible sources of error and ways to minimize these errors are briefly

discussed below. Greatest inaccuracy in estimating D will occur when the reflectivity is near a maximum or minimum on the curve of $\log_{10}(R_{power})$ vs. D, since in these maxima and minima regions the reflected light intensity will be much less sensitive to changes in the film thickness. This error can be reduced by restricting measurements to those regions on the $\log_{10}(R_{power})$ vs. D curve that are not in the vicinity of maxima or minima. Another possible way of reducing this error is to use shorter wavelengths[22] thereby causing the maxima and minima to be narrower. A second source of error is that the sample holder may move due to thermal expansion and thus not permit the full laser beam to shine into the 1/4" i.d. tube attached to the photomultiplier. This error was corrected for by mounting photomultiplier #2 on an x-y micromanipulator which can be adjusted to compensate for the movement of the laser beam. A third source of error is inaccurate measurement of the angle of incidence. This error was reduced by a method of replacing the sample by a rotating mirror and measuring the angle through which the mirror must be rotated to make the laser beam move from being reflected back into the laser to being reflected into photomultiplier #2. Figure 3.3 shows a photograph of the angle measuring device which can be read to 0.4 degree accuracy. A fourth source of error is incorrect polarizer adjustment. In this investigation S-light was used and the beam splitter was positioned so that its plane of incidence was parallel to the sample plane of incidence. For the range of film thicknesses in which the polarizer was adjusted the sample had a larger power reflection coefficient for S-light than P-light. Also the decrease in the power transmission coefficient of the beam splitter when going from P-light to S-light was much less than the increase in the power

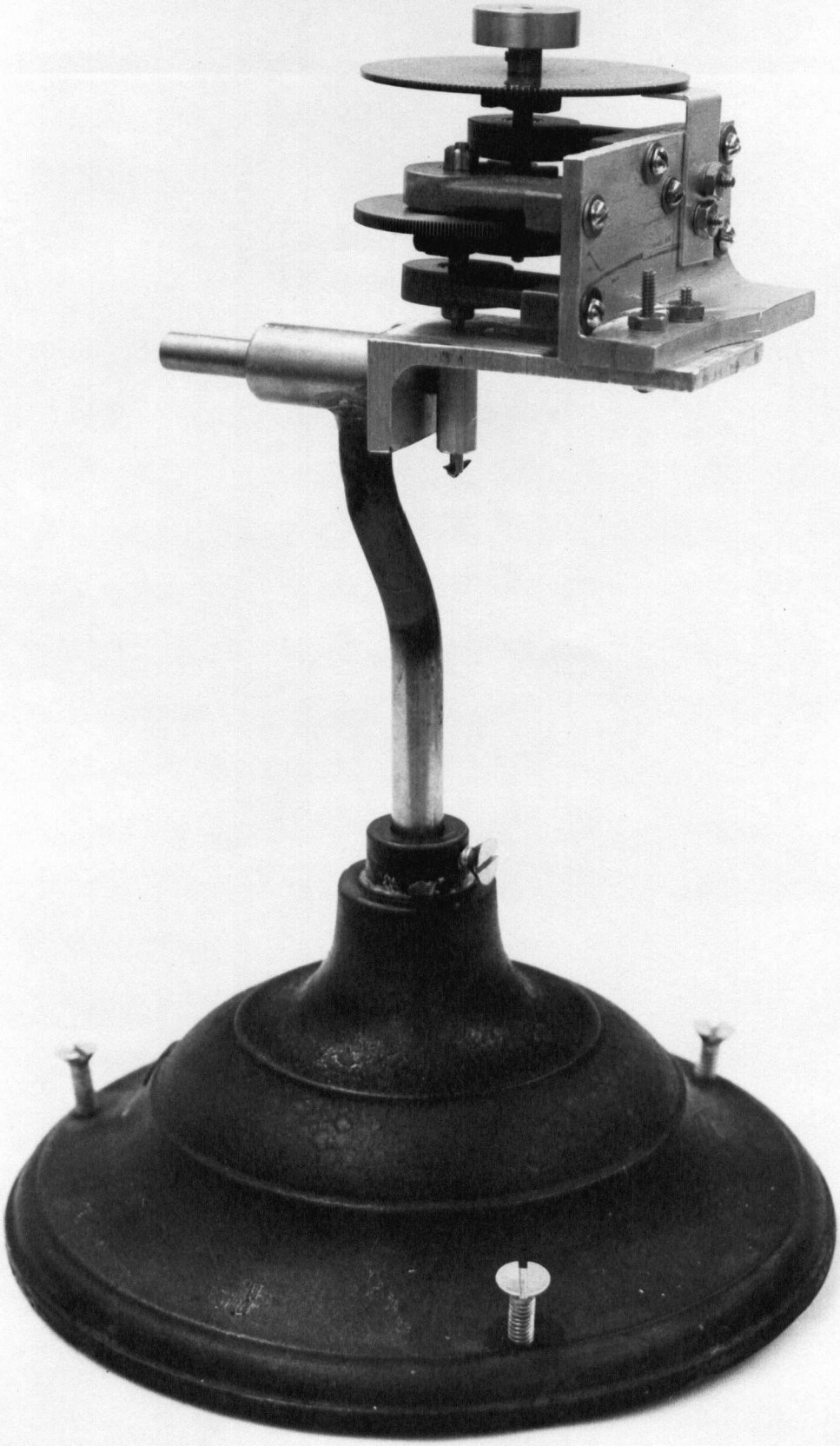

Fig. 3.3

reflection coefficient of the sample in going from P-light to S-light. Thus when S-light was present maximum signal amplitudes were obtained from photomultipliers #1 and #2. A fifth source of error is an incorrect value of refractive index of the substrate. The value of refractive index of the substrate was interpolated from a table of refractive index vs. wavelength[15]. A sixth source of error is a non-linear intensity response of the photomultipliers, but for the fixed wavelength used the photomultipliers had good linearity over the intensity levels used.

2. The discharge cell, sample holder and anodization circuit

The construction of the apparatus is shown in Fig. 3.4. The quartz discharge tube has side-arms with optically flat windows positioned at angles of approximately 36^{o} with respect to the discharge tube axis. Stainless steel end caps, with viton 'O' ring seals, allow sorption pumping of the system at one end and oxygen and sample holder entry from the other. Figure 3.5 shows a detailed drawing of the water-cooled sample holder and temperature measuring thermocouple. An octal header feedthrough allows connection of the sample to the anodizing circuit of Fig. 3.6. This circuit permits the switching from constant current to constant voltage operation and also a continual measurement of the current drawn by the sample. A silicon electrode at ground potential was used as the anodizing current return electrode.

The r.f. power to the plasma is coupled in from a Philips PH1012-02-10-20 model, 12KW, 0.5-1.0MHz, generator by a two turn water-cooled coil around the quartz tube. It is conceivable that the growth conditions could be changed to a considerable extent by using alternative coupling arrangements, but this possibility was not investigated in this thesis.

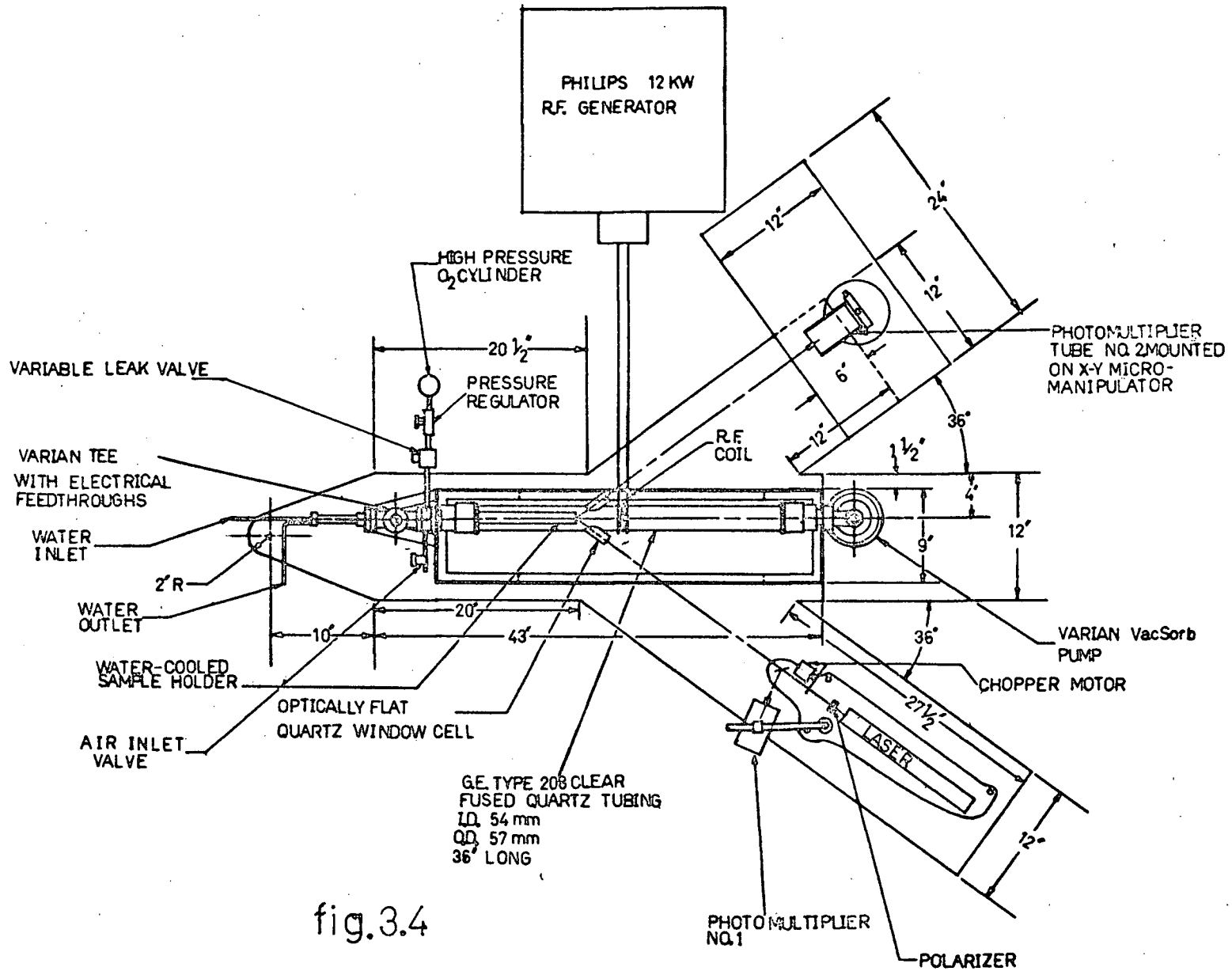
PHILIPS 12 KW
R.F. GENERATOR
HIGH PRESSURE
O_2 CYLINDER
20 ½"
PRESSURE
REGULATOR
VARIABLE LEAK VALVE
VARIAN TEE
WITH ELECTRICAL
FEEDTHROUGHS
WATER
INLET
2"R
WATER
OUTLET
10"
20"
43"
WATER-COOLED
SAMPLE HOLDER
OPTICALLY FLAT
QUARTZ WINDOW CELL
AIR INLET
VALVE
G.E. TYPE 208 CLEAR
FUSED QUARTZ TUBING
I.D. 54 mm
O.D. 57 mm
36" LONG
R.F.
COIL
12"
24"
12"
6"
12"
PHOTOMULTIPLIER
TUBE NO. 2 MOUNTED
ON X-Y MICRO-
MANIPULATOR
36°
1½"
4"
12"
9"
36"
VARIAN VacSorb
PUMP
CHOPPER MOTOR
27½"
LASER
12"
PHOTOMULTIPLIER
NO. 1
POLARIZER

fig. 3.4

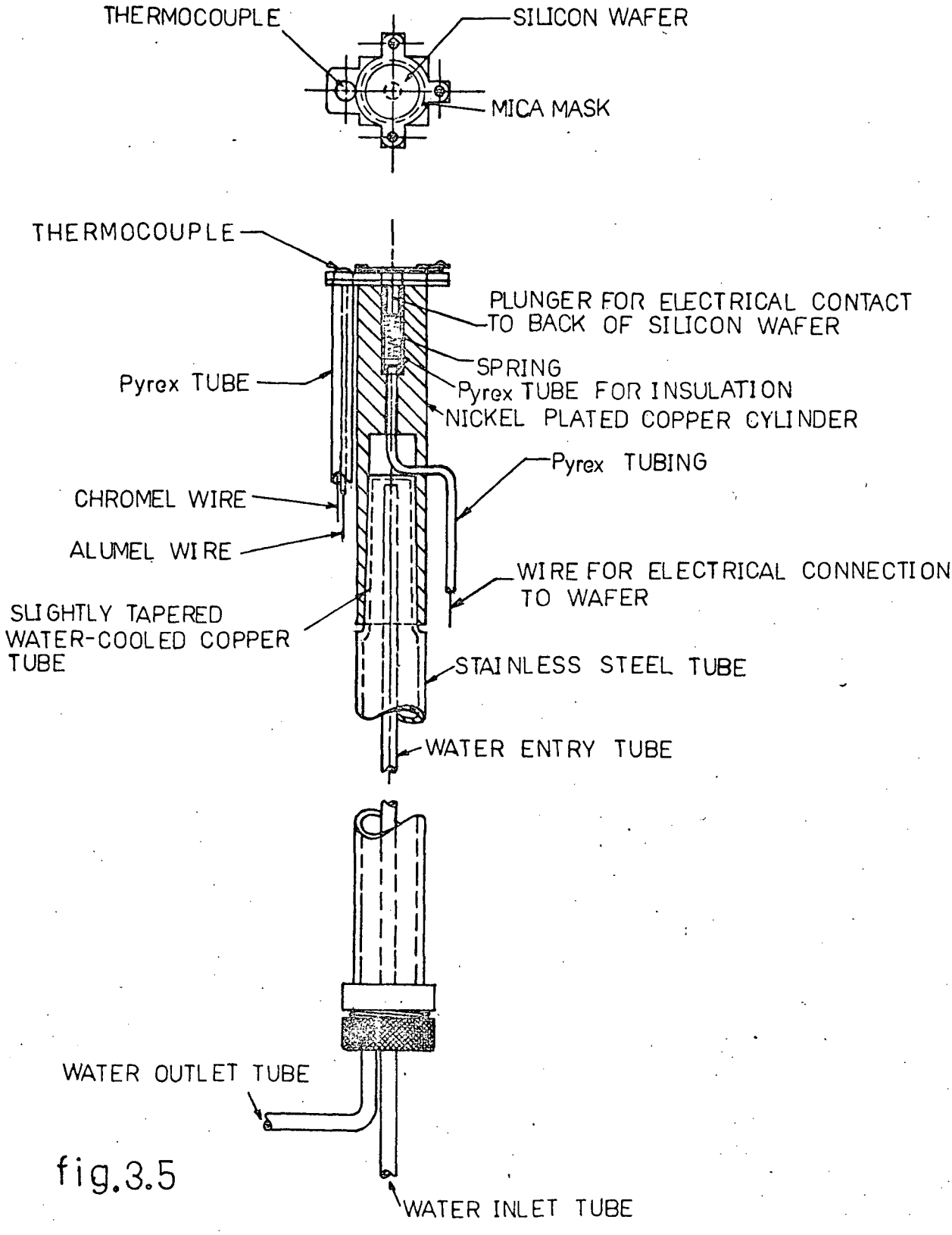
THERMOCOUPLE
SILICON WAFER
MICA MASK
THERMOCOUPLE
PLUNGER FOR ELECTRICAL CONTACT TO BACK OF SILICON WAFER
SPRING
Pyrex TUBE
Pyrex TUBE FOR INSULATION
NICKEL PLATED COPPER CYLINDER
Pyrex TUBING
CHROMEL WIRE
ALUMEL WIRE
WIRE FOR ELECTRICAL CONNECTION TO WAFER
SLIGHTLY TAPERED WATER-COOLED COPPER TUBE
STAINLESS STEEL TUBE
WATER ENTRY TUBE
WATER OUTLET TUBE
WATER INLET TUBE

fig.3.5

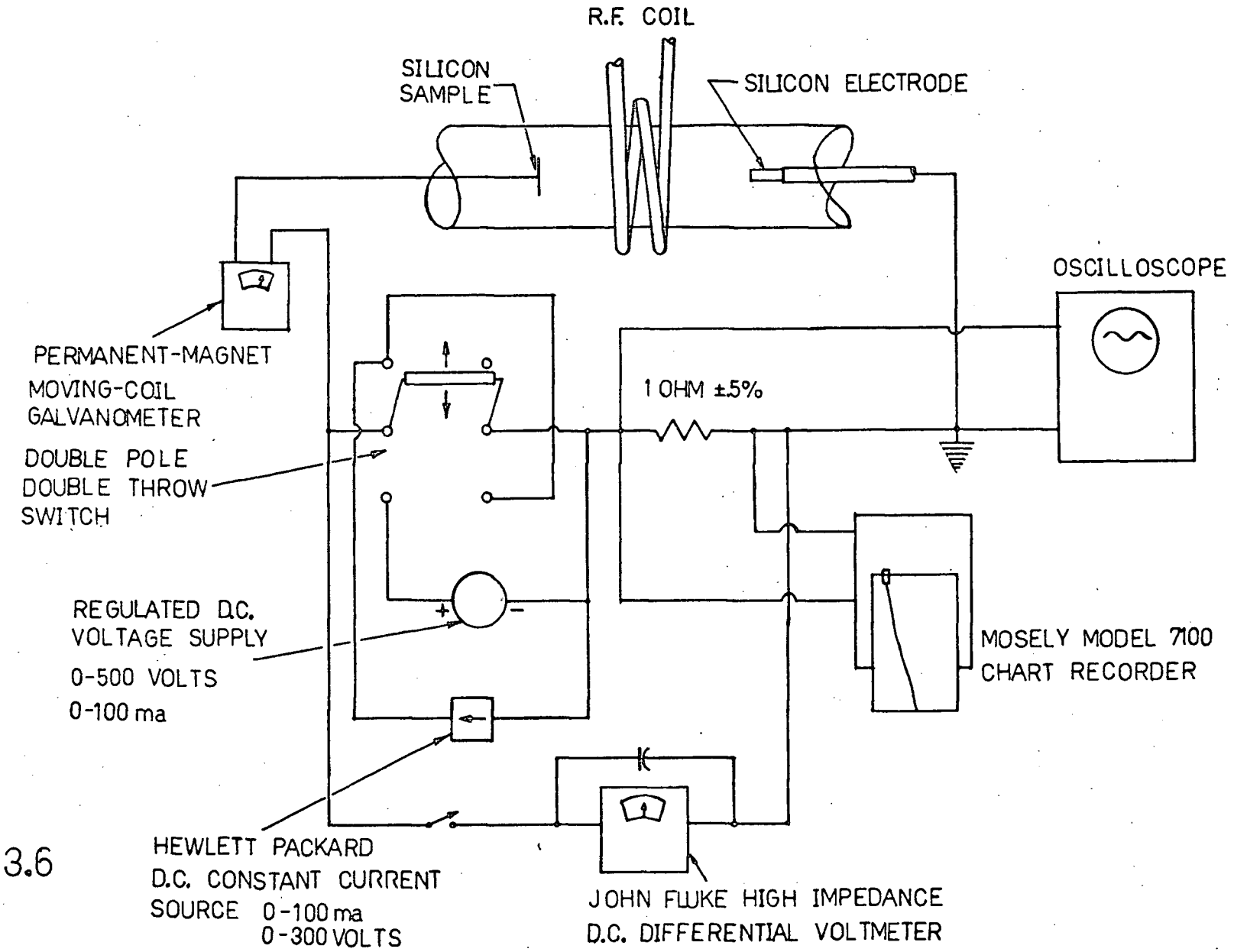
R.F. COIL
SILICON SAMPLE
SILICON ELECTRODE
OSCILLOSCOPE
PERMANENT-MAGNET MOVING-COIL GALVANOMETER
1 OHM ±5%
DOUBLE POLE DOUBLE THROW SWITCH
REGULATED D.C. VOLTAGE SUPPLY
0-500 VOLTS
0-100 ma
MOSELY MODEL 7100 CHART RECORDER
HEWLETT PACKARD D.C. CONSTANT CURRENT SOURCE 0-100 ma 0-300 VOLTS
JOHN FLUKE HIGH IMPEDANCE D.C. DIFFERENTIAL VOLTMETER

fig.3.6

3. Sample preparation

The specimens that were anodized were silicon wafers having n-type impurity concentrations of $3 \times 10^{15}/cm^3$. The wafers, purchased from Monsanto, had been polished by an electrochemical technique to mirror finish. Onto the unpolished back sides of the wafers was evaporated gold doped with 1% antimony. The gold-antimony was then alloyed into the silicon at 425°C in nitrogen with a flow rate of 1000 c.c. per hour for 5 minutes in order to make an ohmic contact. The wafers were cleaved to a size that would fit the sample holder and were then mounted to the sample holder between two mica sheets, the sheet on the polished side of the wafer having a hole in it which exposed the required area (usually 1-2 cm^2).

IV EXPERIMENTAL PROCEDURE

1. Setting up the optical system

The sample holder was positioned a distance of 6" from the r.f. coil; this caused the sample to be in the weaker outer edge of the plasma for pressures in the range of 25-35 millitorr when the generator output was 2 kilowatts.

The laser beam was aligned to give a reflected beam into photomultiplier #2. The VacSorb pump was then opened to the system, pumping it down to 10 millitorr. The variable leak valve was then opened to allow flushing of the system with oxygen for about 15 minutes. The pressure was then reduced to about 30 mtorr and the r.f. discharge was struck with the initial aid of a Tesla coil. The system was allowed to reach a state of thermal equilibrium which was determined by observing when the sample holder temperature, measured by the thermocouple, reached a constant value and also when thermal expansion of the sample holder tube

ceased (i.e. when the x-y micromanipulator no longer required adjustment).

After reaching thermal equilibrium the pressure was adjusted to 32 millitorr where it was kept constant throughout the entire experiment. The x-y micromanipulator was again adjusted to obtain a maximum output from photomultiplier #2. This adjustment was necessary to compensate for any possible movement of the sample holder due to a change in pressure.

The polarizer was then adjusted to obtain maximum signals from photomultipliers #1 and #2 which corresponds to the condition of S-light. The polarizer was adjusted twice, the first time without the beam splitter in the optical system and the second time with the beam splitter present; the reason being to see if the beam splitter would lead to an erroneous adjustment of the polarizer if it were not aligned with its incident plane perfectly parallel to the plane of incidence of the sample. There was no noticeable difference between the two adjustments of the polarizer. The quartz windows did not interfere with the polarizer adjustment since the laser beam was practically at normal incidence to the windows and at normal incidence S-light and P-light are indistinguishable. Decade voltage divider #1 was adjusted to give a reference signal pulse amplitude of about 20 or 25 mV. Decade voltage divider #2 was then adjusted for a null, of the reference and reflected signals, on the differential oscilloscope. These waveforms are shown in Figures 4.1a through 4.3b. Figures 4.1a and 4.1b show the rectangular wave voltages at the inputs #1 and #2 to the differential oscilloscope. Figure 4.2 shows the voltage waveform on the differential oscilloscope when $v_{01} \neq v_{02}$ for the case where F_2 has deviated from its balanced value by 0.035. Figures 4.3a and 4.3b show the voltage waveform on the differential

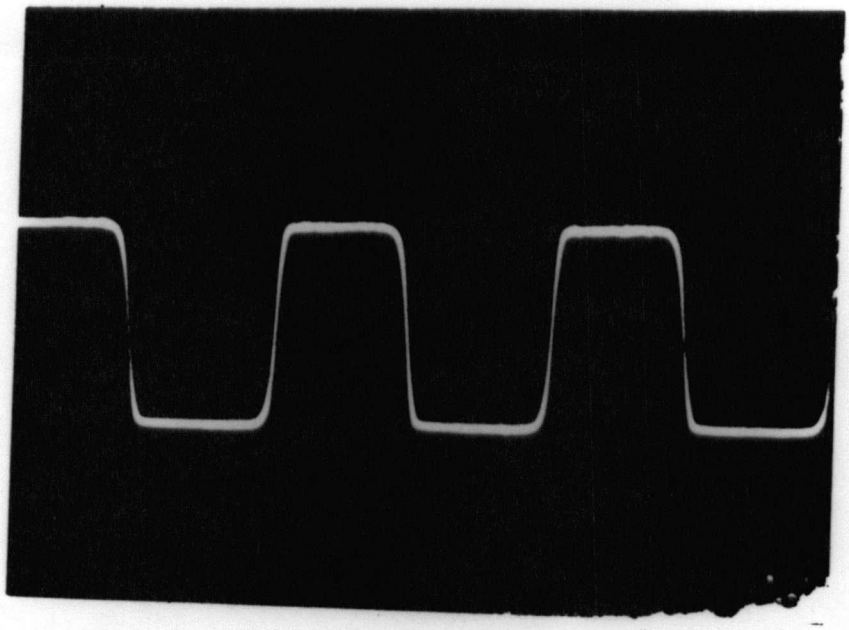

fig.(4.1a) reference signal
sensitivity 5mv/cm

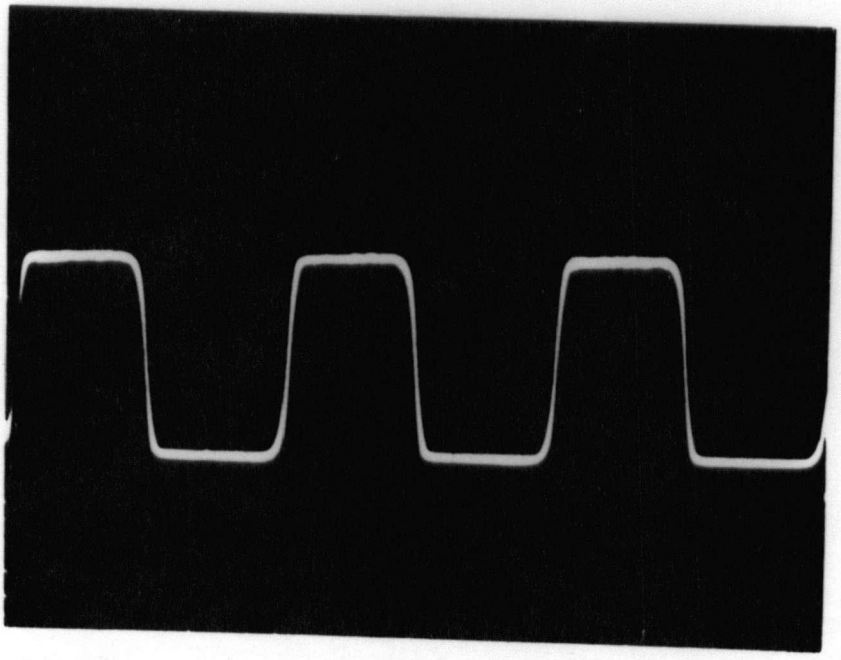

fig.(4.1b) reflected signal
sensitivity 5mv/cm

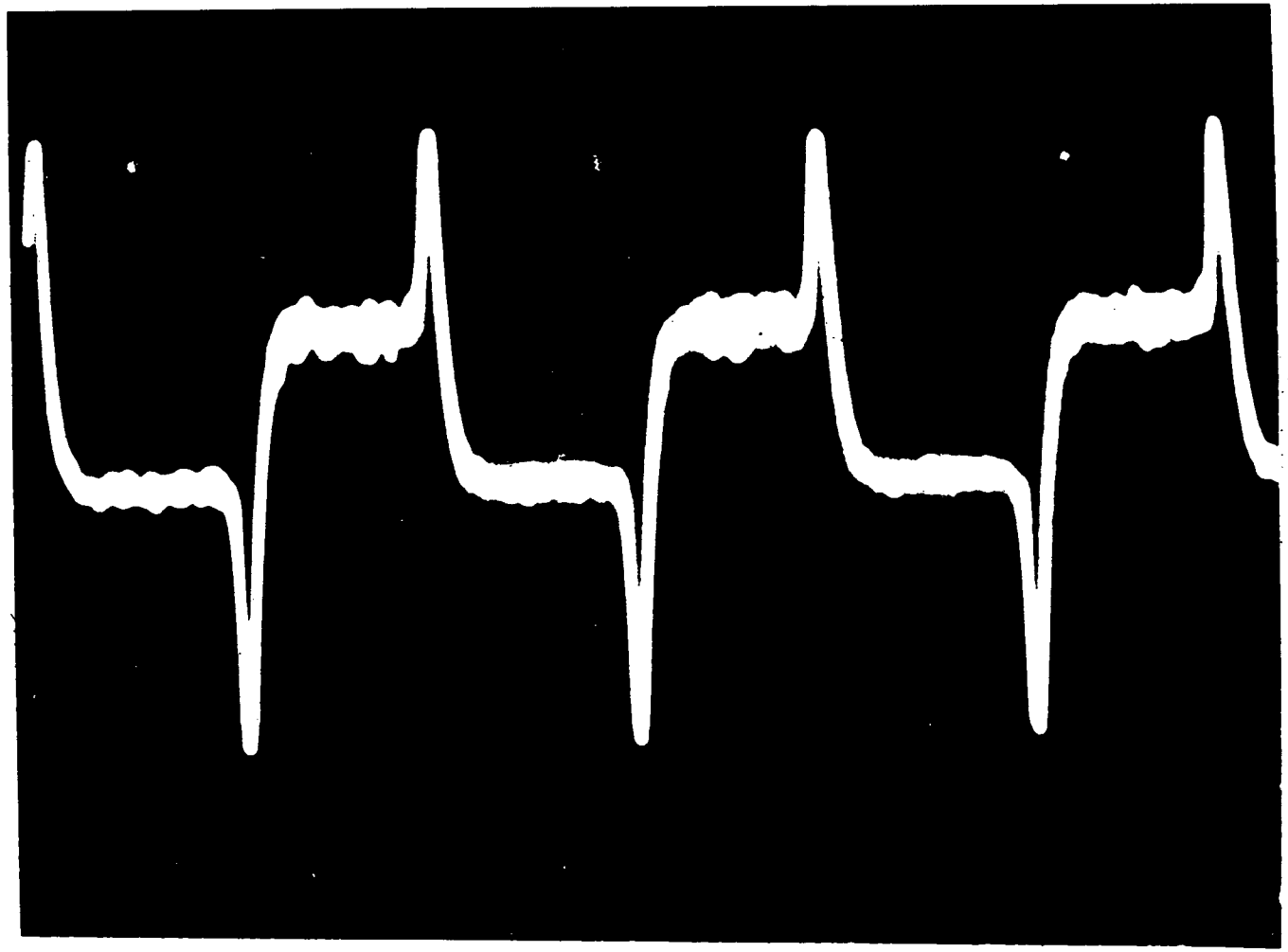

fig.(4.2) sensitivity 1mv/cm

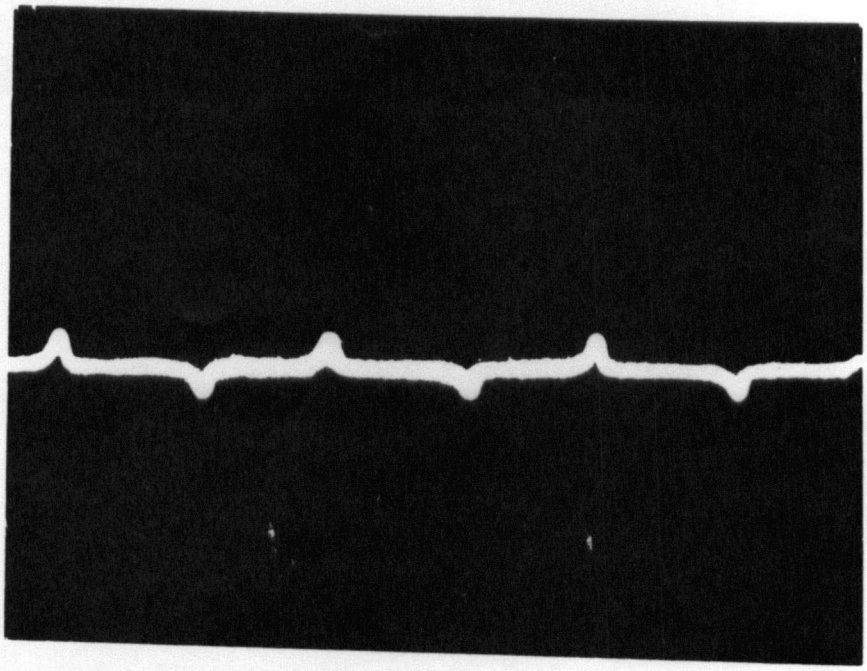

fig.(4.3a) sensitivity 5mv/cm

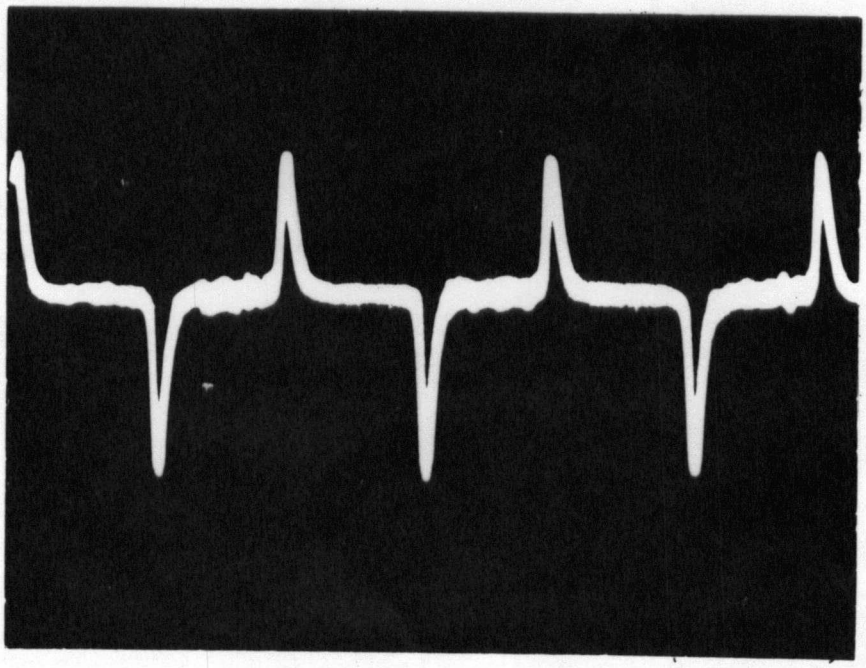

fig.(4.3b) sensitivity 1mv/cm

oscilloscope for the case of a balance where $v_{01} = v_{02}$ for two different voltage sensitivities.

2. Sample temperature measurement

The sample temperature was estimated by the use of a chromel-alumel thermocouple having a reference junction at $0^{o}C$. Figure 3.5 shows the location of the thermocouple next to the sample holder. The thermocouple reading when thermal equilibrium was reached was $200^{o}C$. Thus it can be inferred that the substrate temperature was also approximately the same. Furthermore the spring that made the electrical contact to the silicon substrate did not loose its elastic properties indicating that its temperature remained below $200^{o}C$.

3. Anodization at constant voltage

The sample, which had been electrically floating during the time when the system was reaching thermal equilibrium, was allowed to draw a small constant current of about 1 to 2 ma. The current as a function of time was recorded on a chart recorder. The current was increased in constant current steps of about 3 to 4 ma to a final value of usually around 12 ma. The film was grown at constant current until it reached a thickness that passed the first minima on the curve of $\log_{10}(R_{power})$ vs. D i.e. so that the constant of the optical system could be evaluated, so that the first maxima could probably be reached even if the film grew very little under constant voltage and to be in the range of highest accuracy. After passing the first minima of reflected intensity the sample was switched to constant voltage. The value of constant voltage applied, 129 volts for results presented here, was the value of voltage measured across the terminals of the constant current

generator at the time it was switched to constant voltage. In switching from constant current to constant voltage there was a transient increase in current of 0.6 ma, which was probably due to error in measuring the voltage across the constant current source before switching. The current measured with a permanent-magnet-moving-coil galvanometer* was in good agreement with that as measured on the chart recorder. This suggests that the chart recorder was responding only to the d.c. anodizing current being drawn and not just to some level which might include a rectified component of the r.f. voltage. This check was necessary as an oscilloscope, connected across the one ohm resistor used to measure the current, showed an a.c. signal at the frequency of the r.f. generator with a peak amplitude of 1.5 ma.

The recorded anodizing current decayed slowly with time which was contrary to the current decay for solution grown films[12]. This suggested the possibility of large leakage currents masking the actual current decay. This was later checked by masking off the front face of the sample and applying the same constant voltage that had been applied during constant current growth. Only a small leakage current of .8 ma was measured. This value of leakage current was subtracted from all the values of current measured on the chart recorder thus typically giving an initial current when constant voltage was applied of 12 ma.

As the film grew the optical system became unbalanced and was nulled with decade voltage divider #2 each time the imbalance became large enough to require a .01 to .02 change in the decade voltage divider reading in order to re-establish balance. The values of F_1 and F_2 were

---

* The PMMC galvanometer has essentially zero frequency range.

recorded along with the time when the balance was made. It was possible to see the interference colours of the oxide film through the quartz tube. These colours changed as the film grew and were recorded along with F_1 and F_2 for different times. The films were grown to thickness of about 3800Å. The film thicknesses when constant voltage was applied were about 1400Å with growth rates of about .277 Å/sec. The final growth rates were about .088 Å/sec.

The angle of incidence of the laser beam was measured by the method described in Chapter II.

4. Double probe measurements

To use the probe technique, explained in the appendix, the silicon wafer was removed from the sample holder and replaced by a stainless steel disc masked off to the same surface area as that of the oxide film. The stainless steel disc was biased for a series of values of voltages with respect to the grounded electrode and the d.c. current through the external circuit was measured. The same pressure and power conditions were used during this measurement as were used during the constant voltage growth of the SiO_2 films.

V. EXPERIMENTAL RESULTS

1. Reflectivity data

From the measured values of F_1 and F_2 $\Delta \log_{10}(\frac{F_1}{F_2})$ was calculated to be .682. Using the measured angle of incidence, $\phi_o = 34.4^o$, and the value of the refractive index of the substrate, interpolated from a table of refractive index vs. wavelength[15] ($n_2 = 3.86 - j.017$ for $\lambda = 6328$Å), the refractive index of the film was calculated, by the

method of Chapter III, to be $n_1 = 1.428$. The usual range of refractive index for SiO_2 films ranges from 1.43 to 1.46[17]. Using the value of n_1 the constant of the optical system was determined to be 0.299. The optical constant was subtracted from all the values of $\log_{10}(\frac{F_1}{F_2})$. An enlarged graph of $\log_{10}(R_{power})$ vs. D was made having a modulus of the ordinate of 50 cm/unit and a modulus for the abscissa of .1 millimeter/Å. The values of $\log_{10}(\frac{F_1}{F_2}) - .299$ were placed on this graph along with their corresponding values of time. A photographic reduction of this graph is shown in Figure 5.1.

2. Ionic current density as a function of time and film thickness

From the information contained in Figure 5.1 a large graph of D vs. t was made starting from the time when the constant voltage was applied. The ordinate of the D vs. t curve had a modulus of .1 mm/Å and its abscissa had a modulus of .05 mm/sec. Figure 5.2 shows a photographic reduction of the graph of D vs. t.

The derivative of the D vs. t curve was determined by graphical differentiation using the Chordal Method[16]. The modulus of the ordinate was 400 mm/(Å/sec) and the modulus for the abscissa was .05 mm/sec. Figure 5.3 shows a photographic reduction of the graph of $\frac{dD}{dt}$ vs. t.

By using (2.2), with $\rho = 2.2$ gm/cm^3[17] and M = 60 gm/mole for SiO_2, and the graph of $\frac{dD}{dt}$ vs. t a graph of j_{ion} vs. t was made and is shown in Figure 5.4. In Figure 5.4 the time scale has been changed to minutes with the zero reference corresponding to the instant of switching to constant voltage operation. The total current density was calculated, by dividing the total measured current minus the leakage current (.8 ma) by the area of the sample, and a graph of j_{total} vs. t, for constant voltage

fig. 5.1

PHI = 34.4°
EN1 = 1.428

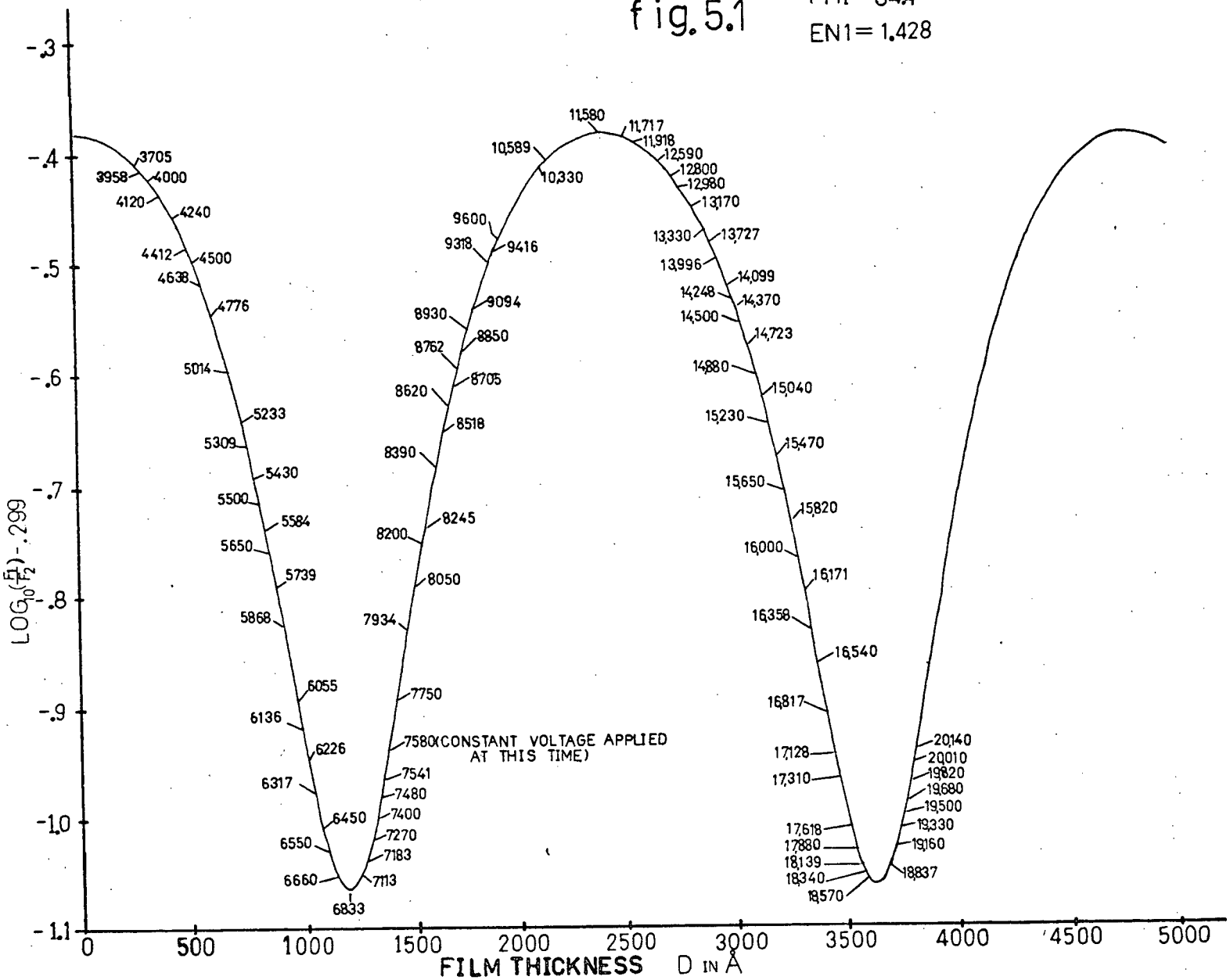

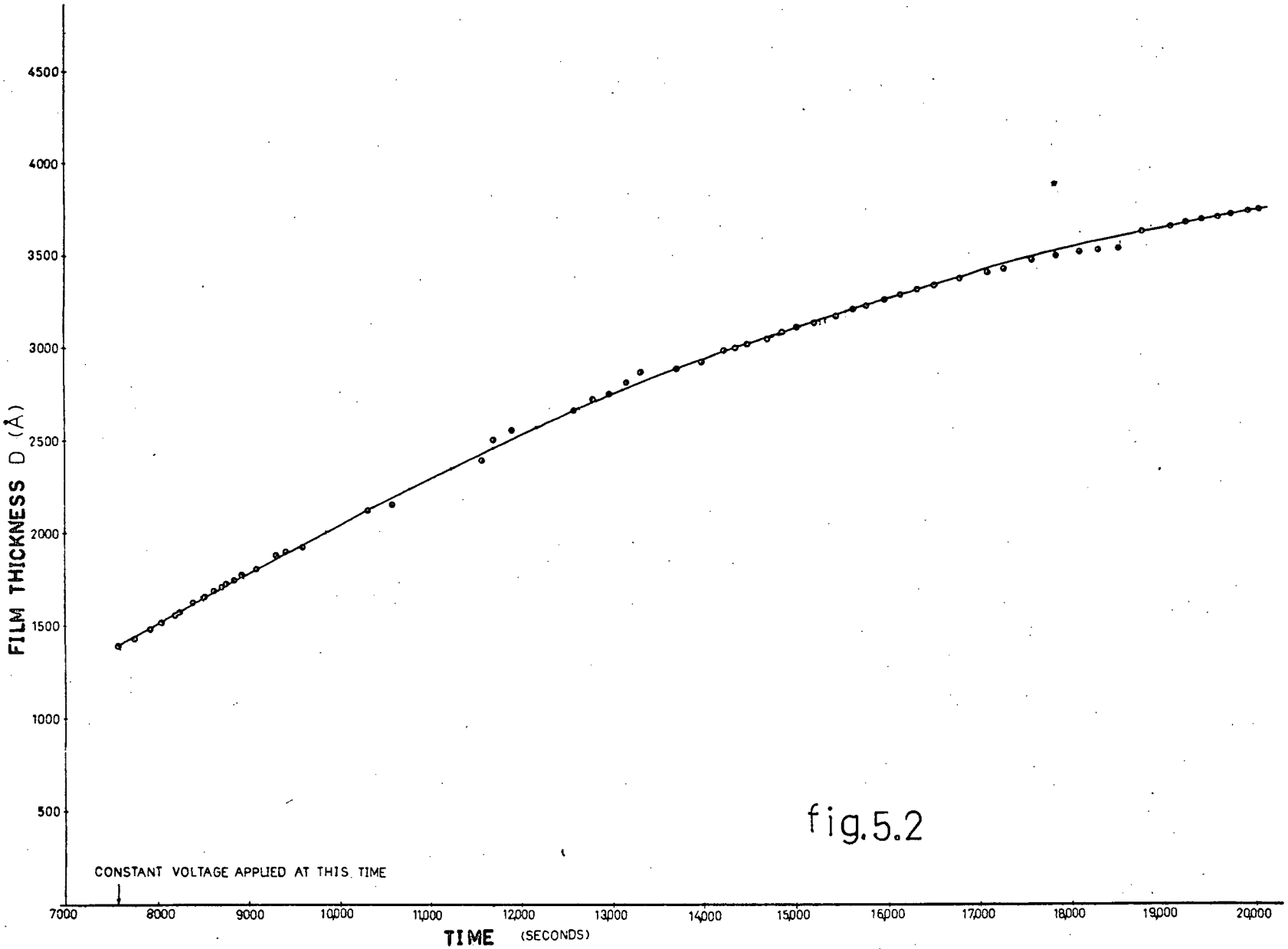
FILM THICKNESS D (Å)
4500
4000
3500
3000
2500
2000
1500
1000
500
CONSTANT VOLTAGE APPLIED AT THIS TIME
7000
8000
9000
10000
11000
12000
13000
14000
15000
16000
17000
18000
19000
20000
TIME (SECONDS)

fig.5.2

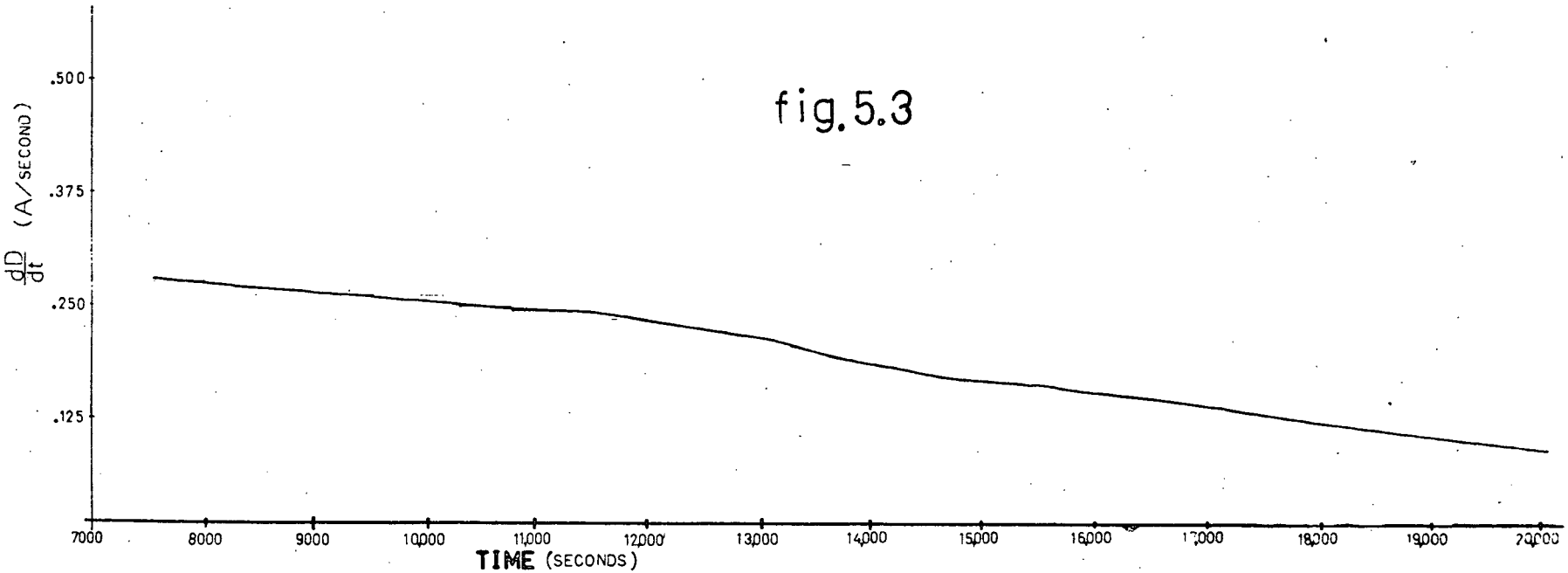
.500
.375
.250
.125
dD/dt (A/SECOND)
7000
8000
9000
10000
11000
12000
13000
14000
15000
16000
17000
18000
19000
20000
TIME (SECONDS)

fig. 5.3

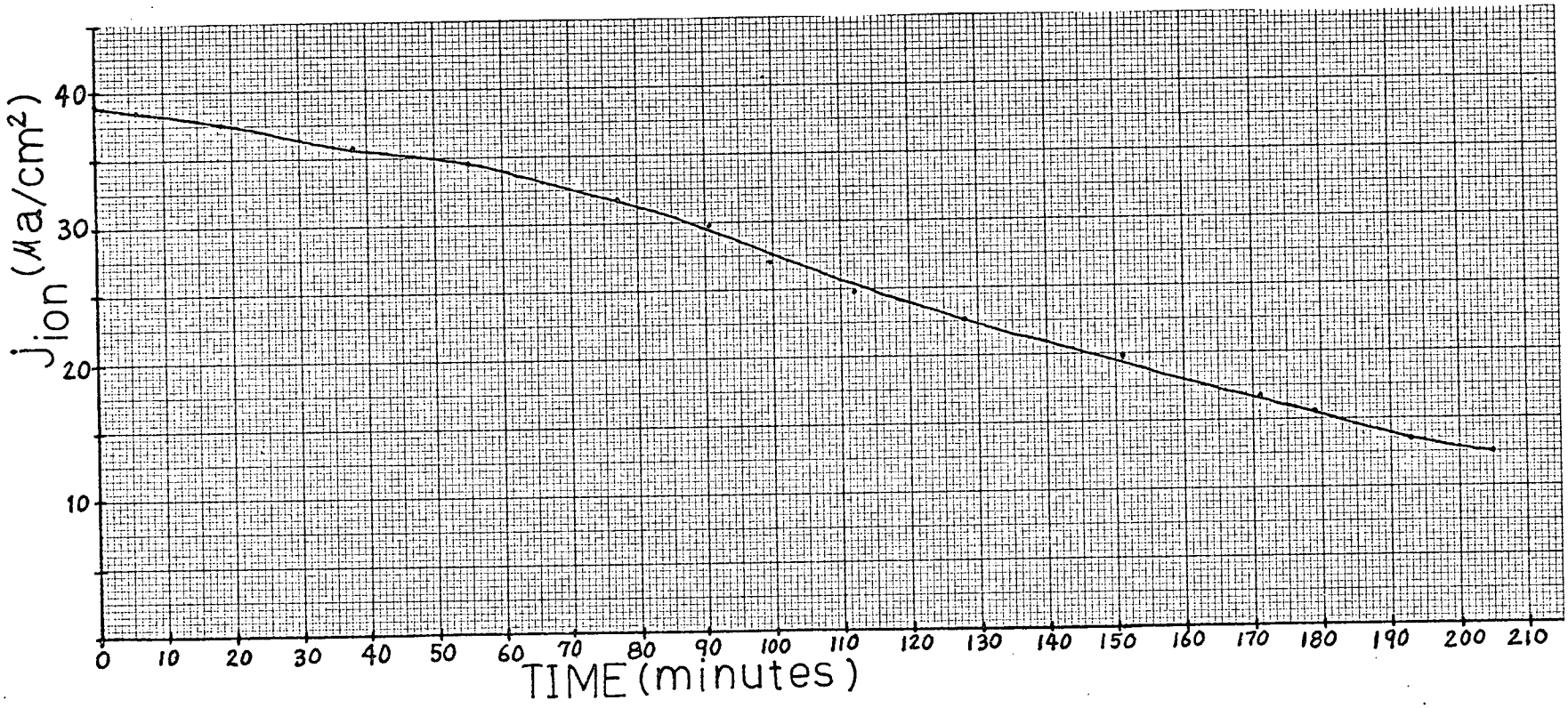
j_{ion} (μa/cm^2)
40
30
20
10
0
10
20
30
40
50
60
70
80
90
100
110
120
130
140
150
160
170
180
190
200
210
TIME (minutes)

fig.54.

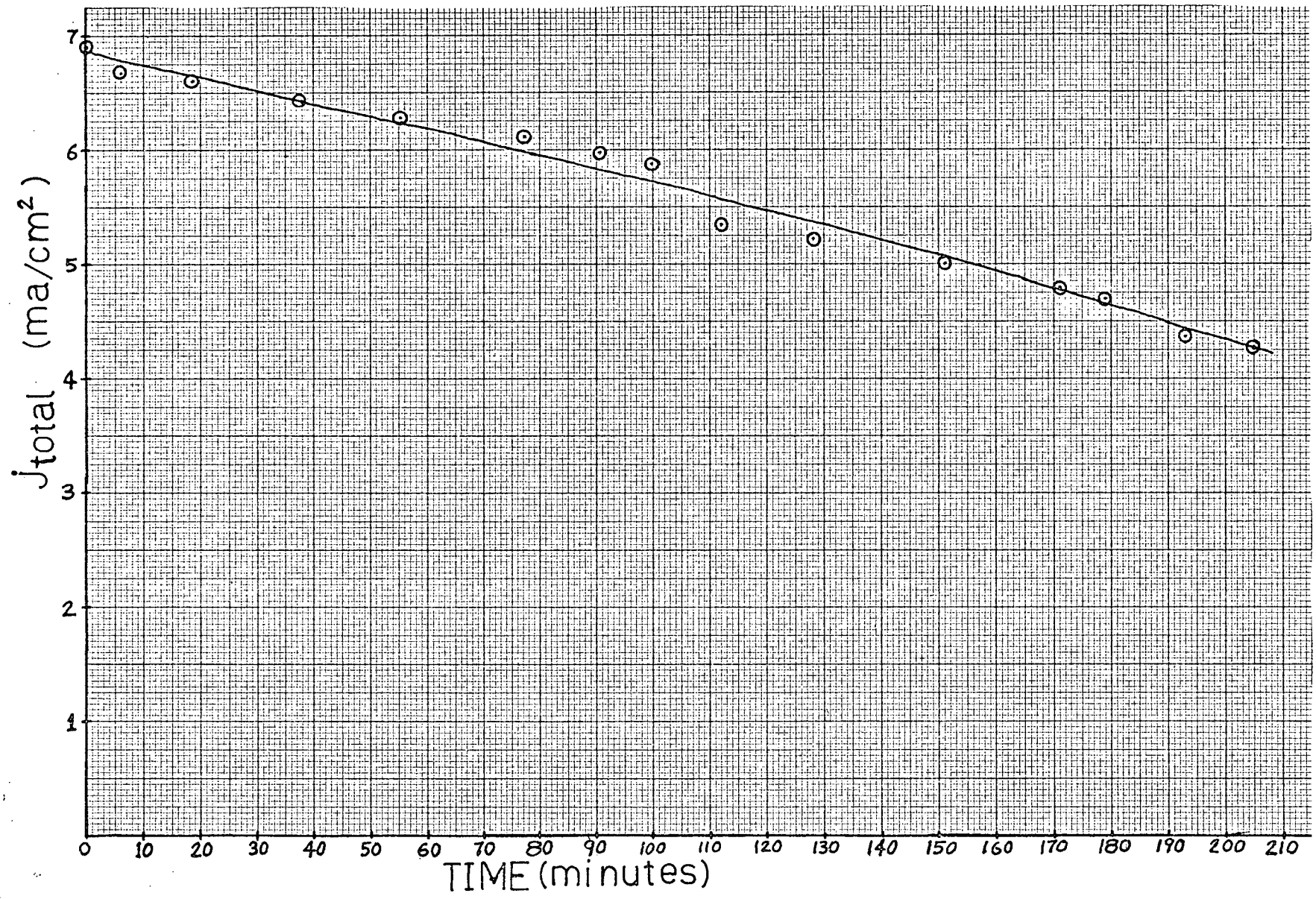
j_{total} (ma/cm²)
7
6
5
4
3
2
1
0 10 20 30 40 50 60 70 80 90 100 110 120 130 140 150 160 170 180 190 200 210
TIME (minutes)

fig.5.5

PT. NO.	TIME SEC.	TIME MIN.	D (Å)	1/D 1/Å	dD/dt Å/SEC.	J ION MICRO-AMPS./CM	J TOTAL MILLI-AMPS./CM	ETA
1	7,700	0.0	1430	7.00E-04	.277	39.20	6.90	5.70E-03
2	8,064	6.1	1530	6.54E-04	.272	38.60	6.67	5.80E-03
3	8,796	18.6	1730	5.78E-04	.265	37.50	6.61	5.67E-03
4	9,987	38.2	2040	4.90E-04	.254	35.90	6.44	5.57E-03
5	11,012	55.2	2300	4.35E-04	.245	34.60	6.29	5.50E-03
6	12,340	77.3	2615	3.83E-04	.225	31.80	6.12	5.20E-03
7	13,133	90.5	2780	3.60E-04	.210	29.75	5.98	4.97E-03
8	13,672	99.6	2890	3.46E-04	.192	27.20	5.86	4.64E-03
9	14,428	112.0	3025	3.31E-04	.175	24.80	5.35	4.64E-03
10	15,404	128.0	3190	3.14E-04	.160	22.60	5.23	4.32E-03
11	16,756	151.0	3400	2.94E-04	.140	19.80	5.00	3.96E-03
12	17,939	171.0	3570	2.80E-04	.118	16.65	4.82	3.46E-03
13	18,441	179.0	3630	2.76E-04	.110	15.60	4.71	3.31E-03
14	19,307	193.0	3720	2.69E-04	.095	13.45	4.37	3.08E-03
15	20,000	205.0	3790	2.64E-04	.088	12.39	4.28	2.90E-03

TABLE 1

operation is given in Figure 5.5.

Fifteen values of j_{total} were taken, for different times during the constant voltage anodization and the current efficiency, η, was calculated for these points. Table I gives the values of D, 1/D, $\frac{dD}{dt}$, j_{ion}, j_{total} and η that correspond to each of the fifteen points. From the points of Table I plots of η vs. j_{total}, j_{ion} vs. 1/D, $\log_{10}(j_{ion})$ vs. 1/D and j_{ion} vs. D were made and are shown in Figures 5.6 through 5.9 respectively.

3a. Calculation of impact ionization theory parameters

j_{leak} and q were calculated using (2.18), (2.19) and different sets of points from Table I. These point sets are listed in Table II along with the corresponding values of j_{leak} and $\frac{q}{a}$ calculated for each point set. Note that j_{leak} and $\frac{q}{a}$ remained reasonably constant over the constant voltage growth range considered, thus justifying the assumption made in Section II.

Table II

Point Set	$\frac{q}{a}$	j_{leak} ma/cm^2
2&11	87.9	3.26
2&15	89.8	3.15
4&11	89.0	3.24
5&10	87.4	3.23
4&13	84.6	3.39

(IONIC CURRENT EFFICIENCY)X10³
1.0
2.0
3.0
4.0
5.0
6.0
7.0
8.0
30
40
50
60
70
80
TOTAL CURRENT DENSITY (MILLIAMPERES/CM²)

fig.5.6

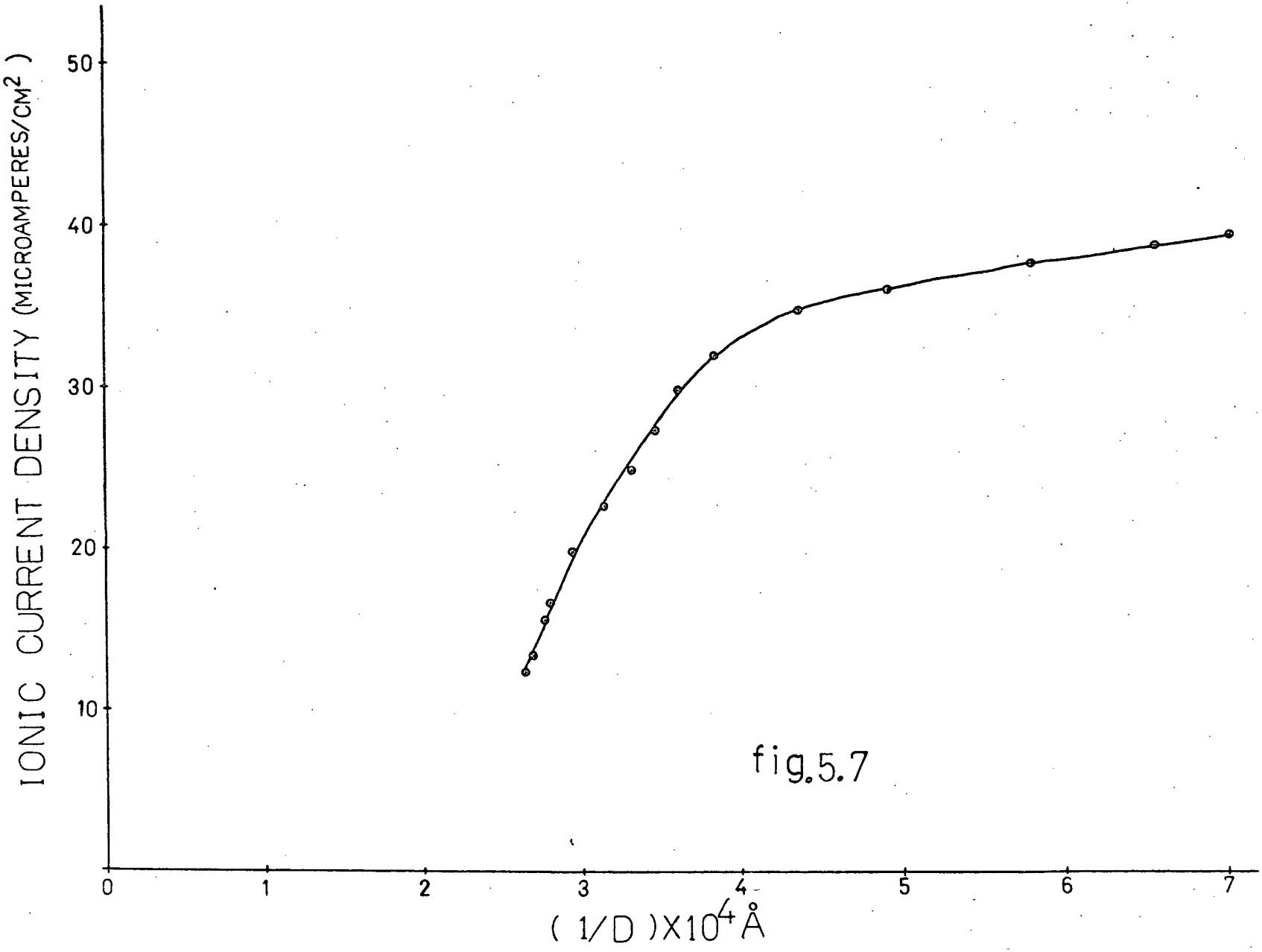
IONIC CURRENT DENSITY (MICROAMPERES/CM^2)
50
40
30
20
10
0
1
2
3
4
5
6
7
(1/D)X10^{4}Å

fig.5.7

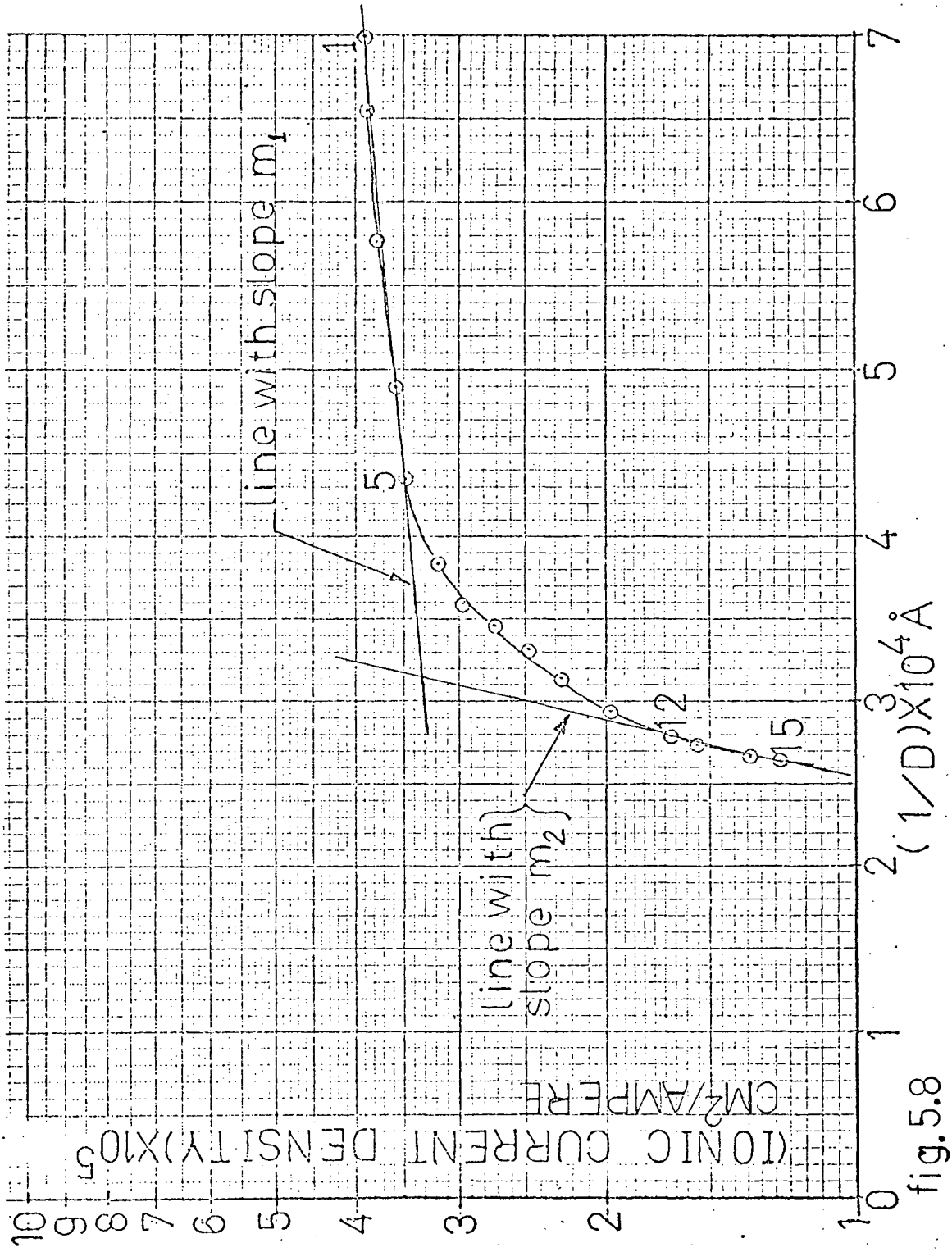
(IONIC CURRENT DENSITY)X10^5
CM²/AMPERE
line with slope m1
line with slope m2
1
5
12
15
(1/D)X10^4 Å^-3
0
1
2
3
4
5
6
7
10
9
8
7
6
5
4
3
2
1

fig. 5.8

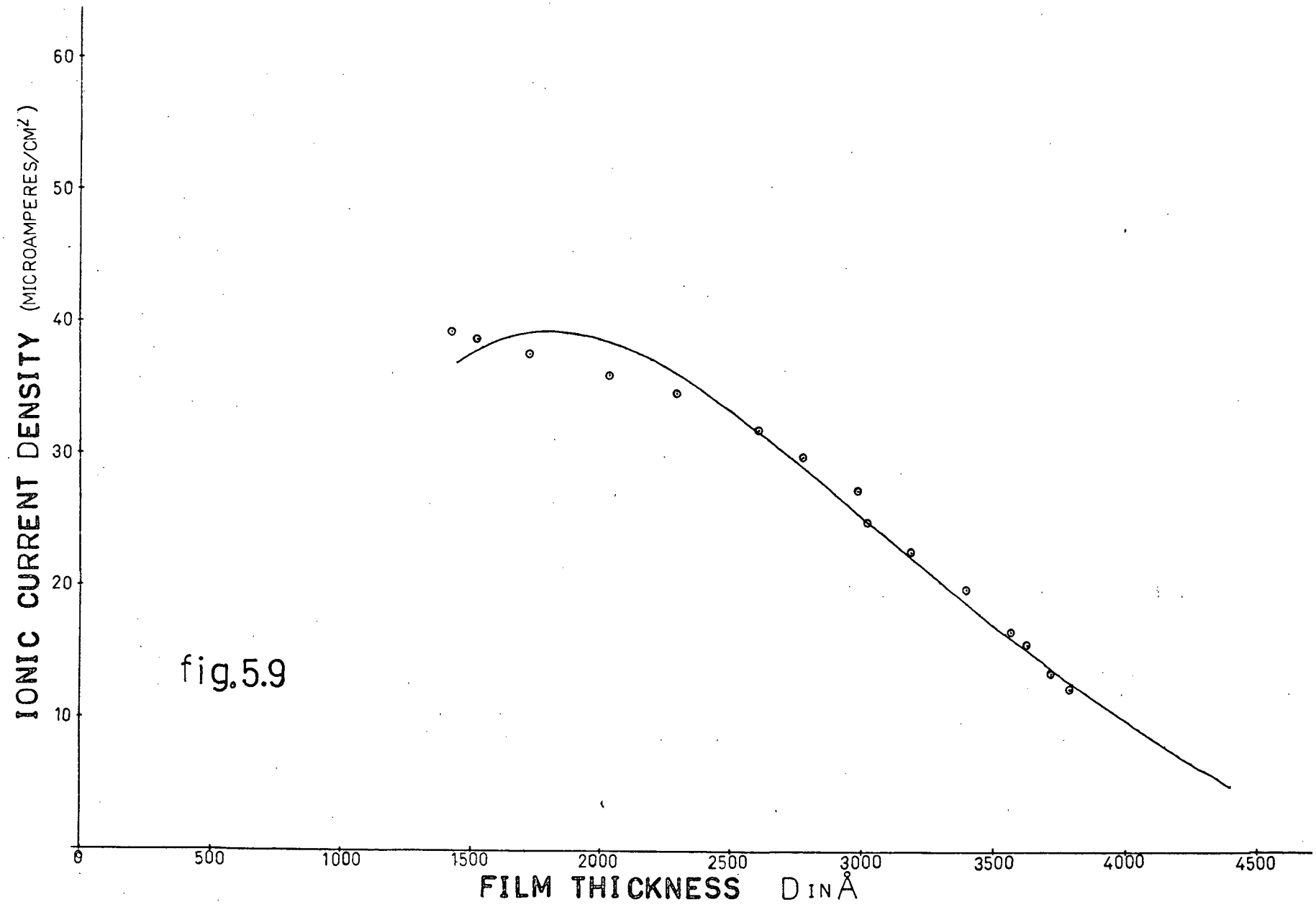
IONIC CURRENT DENSITY (MICROAMPERES/CM²)
60
50
40
30
20
10
0
500
1000
1500
2000
2500
3000
3500
4000
4500
FILM THICKNESS D IN Å

fig.5.9

The average values of $\frac{q}{a}$ and j_{leak} obtained from Table II are $(\frac{q}{a})_{ave} = 87.7$ and $(j_{leak})_{ave} = 3.25$ ma/cm^2. Substituting these values in (2.13) gives the graph shown by the curve in Figure 5.6. Using (2.20), with the average values of j_{leak} and $\frac{q}{a}$, sets of values of (D, vt_i) were calculated for different sets of points from Table I. These calculated sets of (D, vt_i) as well as D/vt_i are listed in Table III along with the corresponding point from which each set was calculated.

Table III

Point	D Å	vt_i Å	D/vt_i
1	1430	700	2.04
4	2040	1030	1.98
6	2615	1380	1.89
7	2780	1500	1.85
11	3400	2100	1.62
15	3790	2680	1.42

Different pairs of the points of Table III were taken two at a time and were substituted into (2.21) and (2.22) from which were calculated μ_{el} and τU. The value of the ionization potential, I, for SiO_2 used in (2.21) and (2.22) was 11 eV. as has been determined by Fritzsche[18] from breakdown measurements on SiO_2 films. Table IV lists the calculated values of μ_{el} and τU taken for five different combinations of sets of points in Table III. Note that μ_{el} and $U\tau$ remain reasonably constant over the constant voltage growth range considered.

Table IV

Pairs of Points	μ_{el} cm^2/volt sec	U_τ volt sec
1&7	27.9	1.98×10^{-12}
1&15	27.7	1.96×10^{-12}
4&15	30.2	2.05×10^{-12}
6&15	28.2	1.98×10^{-12}
4&11	31.6	2.14×10^{-12}

The average values of μ_{el} and $U\tau$ determined from TABLE IV are $(\mu_{el})_{ave}$ = 29.1 cm^2/volt sec and $(U\tau)_{ave} = 2.02 \times 10^{-12}$ volt sec.

3b. Theoretical dependence of ionic current density on thickness for impact ionization

The average values of j_{leak}, $\frac{q}{a}$, μ_{el} and $U\tau$ were substituted into (2.17) and a graph of j_{ion} vs. D was made which is the curve in Figure 5.9. The limiting thickness of the oxide film was calculated by substituting $(\mu_{el})_{ave}$ and $(\tau U)_{ave}$ into (2.24) a graph of which is shown in Figure 5.10. The value of D_{max} was estimated to be D_{max} = 4900 Å while the value of D_{min} was estimated to be D_{min} = 400 Å. It is noteworthy that the latter value was far below the value of film thickness when the constant voltage was applied.

4a. Double probe characteristics

From the probe measurement of Section 4, Chapter IV a graph was made of probe current vs. voltage and is shown in Figure 5.11. The intital total current drawn by the sample was I_1 = 12 ma, obtained from point 1 of Table I by multiplying j_{total} by the area of the sample, and

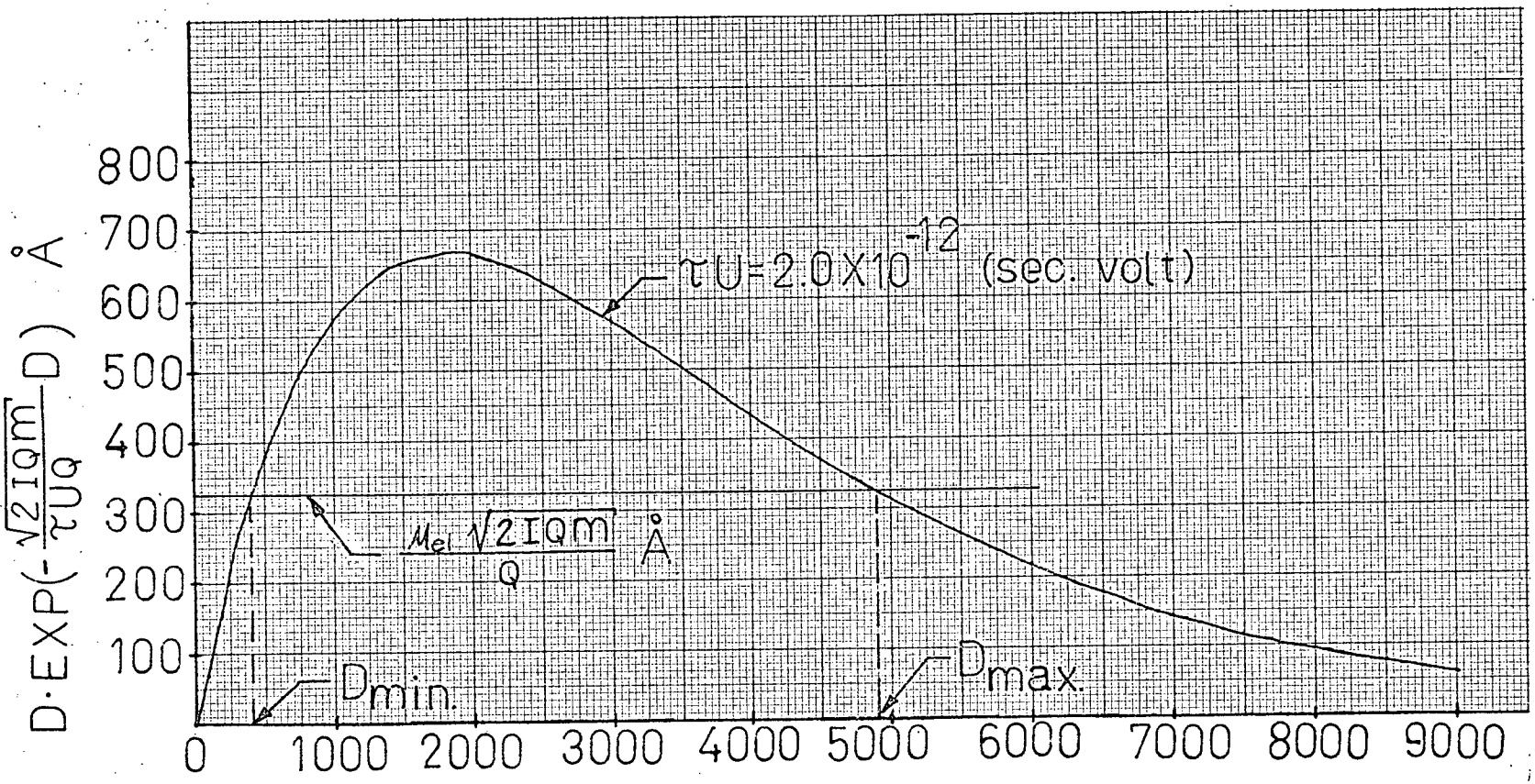
D·EXP(-√2IQm/τUQ D) Å
800
700
600
500
400
300
200
100
0
1000
2000
3000
4000
5000
6000
7000
8000
9000
τU=2.0X10^-12 (sec. volt)
μel √2IQm/Q Å
Dmin.
Dmax.
D (Å)

fig.5.10

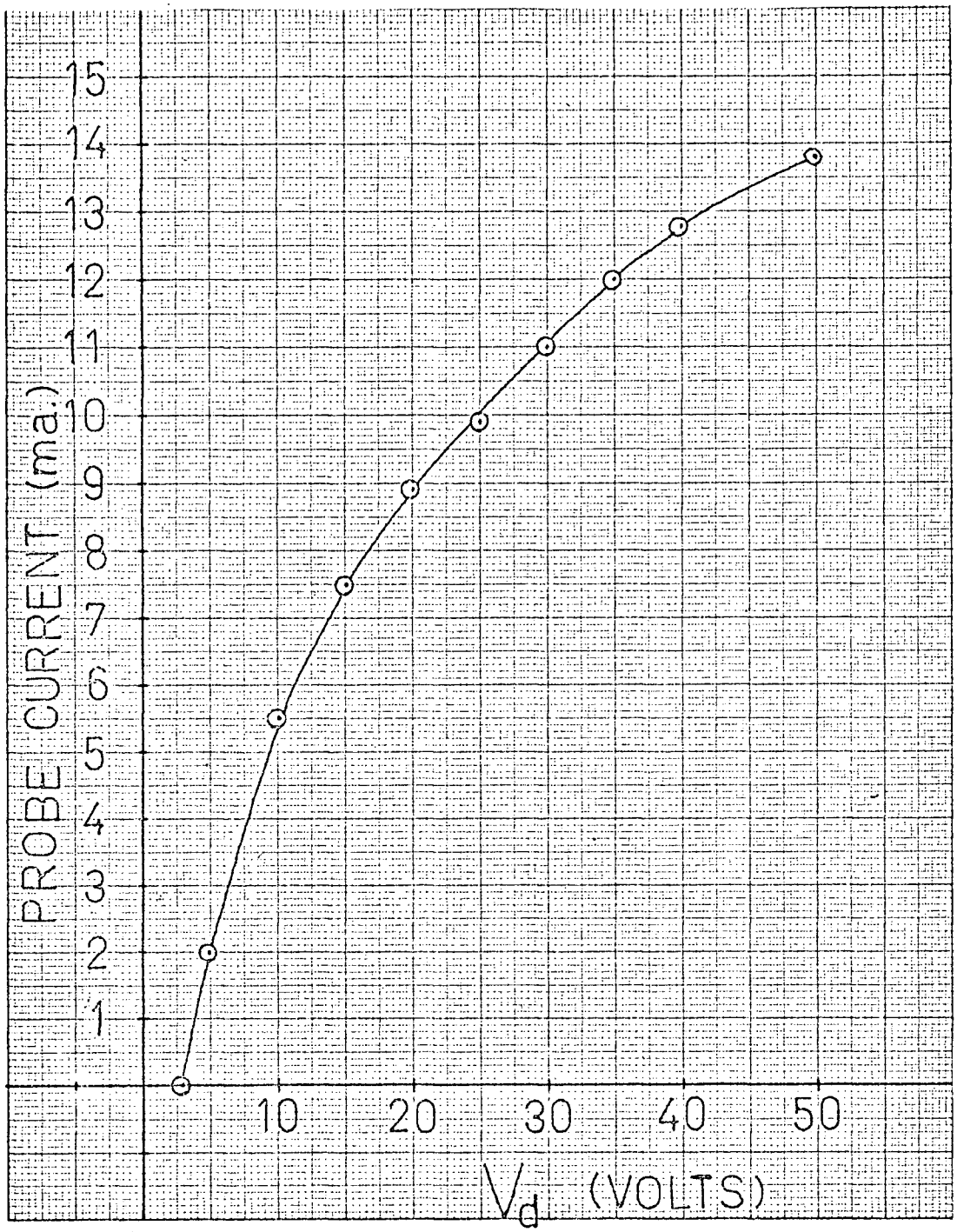
PROBE CURRENT (ma.)
15
14
13
12
11
10
9
8
7
6
5
4
3
2
1
10
20
30
40
50
V_d (VOLTS)

fig.5.11

the final total current was I_2 = 7.45 ma. Thus from Figure 5.11 V_{d1} = 35 volts and V_{d2} = 15 volts (see Appendix).

4b. Comment on the theoretical and actual change in voltage drop and electric field in the oxide under conditions of constant voltage anodization

Using the values of V_{d1} and V_{d2} of Section 4a. Chapter V, the value of V_{supply} (129 volts) and (1) and (2) of the Appendix the initial and final values of the voltage across the oxide are U_1 = 94 volts and U_2 = 114 volts respectively. The percentage voltage regulation was, from (4) of the Appendix, 21%. The value of γ calculated from (10) of the Appendix was 7.92%.

The average velocity of electrons crossing the film can be estimated by using the average value of mobility and the initial value of the electric field ($E_1 = \frac{U_1}{D_1} = 6.57 \times 10^6$ volts/cm). Using the relation $v = \mu_{el} E_1$ the electron velocity v obtained was 1.9×10^8 cm/sec, while the velocity of light is approximately 3×10^{10} cm/sec. Thus $v/c = .006$ and the theory of relativity has not been violated.

VI DISCUSSION

If the rate-limiting diffusion theory is applicable the graph of j_{ion} vs. 1/D, shown in Figure 5.7, should be a straight line given by (2.3). It can be seen from Figure 5.7 that no single straight line can account for the data. A possible source of deviation from a straight line could occur in practice due to a change in the value of the pressure dependent rate constant K, but since the pressure was held constant it appears that the rate-limited diffusion theory does not explain the experimental results.

For high-field ionic conduction, the graph of $\log_{10}(j_{ion})$ vs. $1/D$, Figure 5.8, should be a straight line according to (2.6). Again the experimental data is not accounted for by a single straight line, but as has been pointed out in the Appendix the value of U would increase somewhat as the film grew. The possibility arises therefore that the deviation of the curve in Figure 5.8 from a straight line is due to an increasing voltage with increasing film thickness. Writing (2.6) as

$$y = mx + b \ , \tag{6.1}$$

where $y = \log_{10}(j_{ion})$, $x = 1/D$, $m = BU \log_{10}e$ and $b = \log_{10}J_0$ we have the equation of a straight line of slope m and y intercept b. The curve in Figure 5.8 may be divided up into two straight lines one line from point 1 to point 5 with slope m_1 and another line from point 12 to point 15 with slope m_2. The line from points 1 to 5 is where the voltage has a constant value U_1 and the line from points 12 to 15 is where the voltage has a constant value U_2. The percent voltage regulation during the growth of the film can be expressed in terms of the slopes m_1 and m_2 by (6.2).

$$\text{(percentage voltage regulation)} = \frac{U_2 - U_1}{U_1} \times 100 = \frac{m_2 - m_1}{m_1} \times 100 \tag{6.2}$$

The slopes m_1 and m_2 were calculated giving $m_1 = 204$ units/(Å^{-1}) and $m_2 = 8100$ units/(Å^{-1}). The required voltage regulation to fit the high-field ionic conduction theory is thus 3870%! However the predicted percentage voltage regulation from probe measurements is only 21%. It should also be noted that the two lines have greatly different y intercepts which would mean that the value of b changed greatly during the growth of the film, but this is very unlikely. Thus these results seem to indicate that the high-field ionic conduction mechanism is not responsible

for the growth of SiO_2 films in an r.f. plasma.

Having shown that the rate-limited diffusion theory and the high-field ionic conduction theory are not applicable to this investigation, the impact ionization theory is next considered. The graph of η vs. j_{total}, (2.13), using the values of $(\frac{q}{a})_{ave}$ and $(j_{leak})_{ave}$ agrees well with the experimental points as can be seen from Figure 5.6.

The average value of μ_{el}, calculated from Table IV was 29.1 cm^2/volt sec and it is worth noting that Goodman[19] obtained an average value of 29 cm^2/volt sec for the electron mobility in SiO_2 films using a modified Hall measurement technique especially suited for use with insulator films. The fact that the average value of electron mobility obtained from Table IV is the same as the average value of electron mobility measured by Goodman is a strong factor for suggesting that the impact ionization theory is responsbile for the growth of the film. Furthermore, considering the graph of j_{ion} vs. D (2.17), which is shown in Figure 5.9, it is noted that there is good agreement with the experimental points.

There is thus strong evidence in support of the impact ionization theory as presented here being responsible for the growth process in r.f. plasma anodization of silicon. However it is perhaps of interest to remark on the differences in current decay rate that result from consideration of the above theory and Fritzsche's original theory[12]. Fritzshe derived an equation giving the current density time decay at constant voltage as

$$\frac{1}{j_{total} - j_{leak}} - \frac{1}{j_{total_0} - j_{leak_0}} = B(t - t_0), \qquad (6.3)$$

where the constant voltage was applied at time t_0 when the total current

density was j_{total_0} and the leakage current density was j_{leak_0}. B is a constant independent of voltage. Equation (6.3) was derived for the case of solution anodization of SiO_2 where the assumptions were made that $D/vt_i >> 1$ and that the primary electrons could be neglected. In the present experiment the values of D/vt_i varied from 2.04 to 1.42 which does not satisfy the above requirements. Therefore (6.3) could not be valid for this experiment. The total current density can be written in terms of the leakage current density and the ionic current density as

$$j_{total} = j_{leak} + (1+\frac{q}{a})j_{ion}.$$

By assuming that j_{leak} and $\frac{q}{a}$ are constant one can expect the total current to vary with time in the same manner as the ionic current density varies. The film thickness D can be expressed as a function of time in terms of the ionic current density by (2.2) as

$$D = D_0 + (\text{constant}) \int_{t=0}^{t} j_{ion} dt, \qquad (6.4)$$

where the constant voltage was applied at time t=0 when the film thickness was D_0. If (2.17) is substituted for j_{ion} in (6.4) an implicit function in D is obtained which is difficult or perhaps impossible to solve for D as a function of time. Thus in this investigation no explicit expression has been given for D or j_{ion} as a function of time.

VII CONCLUSION

Silicon dioxide thin films were grown on single crystal silicon wafers by the plasma anodization technique in an r.f. excited oxygen plasma. Film thicknesses were measured in situ by a technique utilizing the variation of the intensity of a laser beam reflected from a growing

film as a function of film thickness. The optical system was so designed that it was possible to make thickness measurements continuously with the plasma on. To elucidate the nature of the growth mechanism films were grown under conditions of constant pressure (~32 millitorr), constant sample temperature (~200°C) and with an anodizing voltage held constant for film growth in the typical thickness range of 1400 Å to 4000 Å. A double probe method was used to estimate the voltage regulation of the voltage across the oxide film with a constant bias voltage applied to the sample and it was found to be 21%. However for the purposes of comparing the experimental data the error in electric field change is more important; this error was only 7.9%.

Three different theories of anodization were investigated: (1) the rate-limiting diffusion theory (2) the classical theory of high-field ionic conduction in solids and (3) the impact ionization theory. Of the three theories proposed, the experimental results strongly indicate that the impact ionization theory is applicable over the film thickness range considered in this experiment. The electron mobility in the SiO_2 film was calculated from the experimental data using the value of ionization potential given by Fritzsche[18] for SiO_2 films, and found to be 29 cm^2/volt-sec which agreed very well with the value determined by Goodman[19] from modified Hall measurements for insulators.

The following is a list of topics suggested for further research:

(a) The verification of the upper limits of oxide film thickness, as predicted by the impact ionization theory, for given sets of conditions.

(b) The optimization of the growth rate by investigation of the effects of gas pressure, position of the sample and type of r.f. power coupling.

(c) The detailed study of the dielectric properties of SiO_2 films grown by r.f. plasma anodization to assess the applicability of this technique to integrated circuit technology.

APPENDIX

The problem of maintaining a constant voltage across the oxide film

The need arose for a method of maintaining a constant voltage, U, across the oxide film while the film was growing. The simpleist biasing arrangement is to apply a constant voltage, V_{supply}, to the sample with respect to the grounded electrode (see Figure 3.6), but this may not necessarily mean that U remains constant. In this Appendix an estimate is made of the constancy of U for a given constant V_{supply}. A method of analyzing this problem is to consider the system of Figure 3.6 as that of a double probe system with one of its probes grounded. Johnson and Malter[20] analyzed the double floating probe arrangement, which differs from the arrangement in this experiment in that here one of the probes is grounded and instead of the potentials on both of the probes changing the plasma potential is forced to move with respect to the grounded probe.

The surface of the oxide film can be considered as probe number (1) having an area, A_1, the same as the surface area of the oxide film. The electrode can be considered as probe number (2) having an area A_2. Figure (1) shows the potential diagram between probes (1) and (2) with a positive potential applied to probe (1) with respect to probe (2) which is grounded. The potential V_c represents the difference in the plasma potentials due to non-uniformity of the plasma.

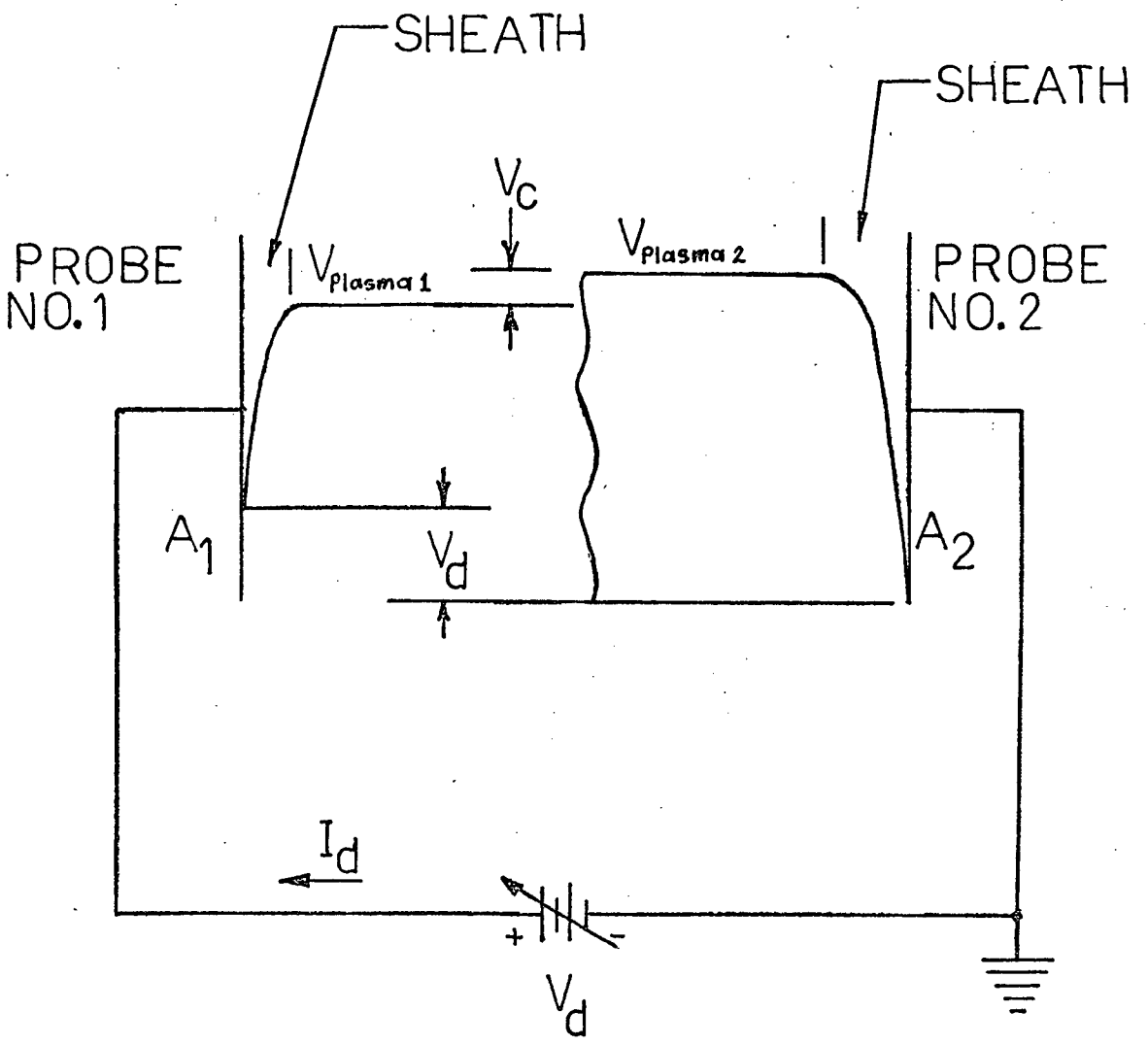
SHEATH
SHEATH
V_c
PROBE NO.1
$V_{Plasma\ 1}$
$V_{Plasma\ 2}$
PROBE NO.2
A_1
V_d
A_2
I_d
+
-
V_d

Fig. (1)

To simplify the analysis of the probes assume that $A_1 = A_2$ and that $V_c = 0$. Furthermore assume that V_d has no effect on the ion current to the probes. This is a reasonable approximation as the heavy ions are much less influenced by a potential on the probe than are the lighter electrons. In order to better understand how the probes work it is worth considering the following five cases.

Case 1 occurs when $V_d = 0$ so that the number of electrons arriving at each probe is the same. The electron current flowing to each probe will balance the positive ion current flowing to each probe and no net current will flow in the external circuit. Figure 2a. shows the potential diagram for case 1.

Case 2 occurs when V_d is a small positive voltage so that probe (1) draws more electrons than probe (2). Since probe (2) is grounded it cannot go more negative in order to make a deficiency of electrons at probe (2) to compensate for the increase in electrons being drawn by probe (1). Thus the electrons drawn from the plasma by probe (1) cause the plasma potential to rise so that probe (2) is now more negative with respect to the plasma potential and thus draws fewer electrons. The excess electrons at probe (1) then flow through the external circuit to probe (2) to compensate for the deficiency of electrons at probe (2) and a net current, I_d, flows through the external circuit. The potential diagram for case 2 is shown in Figure 2b.

Case 3 occurs when V_d is made large and positive. Now probe (1) draws a large number of electrons from the plasma so that the plasma potential is forced quite far upward making probe (2) highly negative with respect to the plasma potential so that probe (2) no longer draws electrons

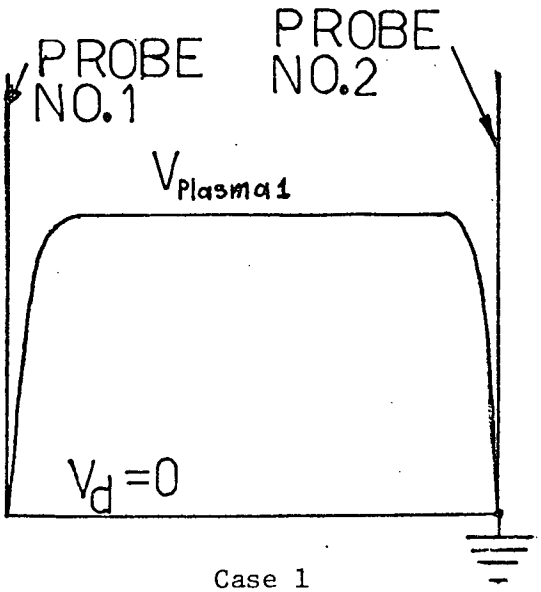

Case 1

Fig. 2a

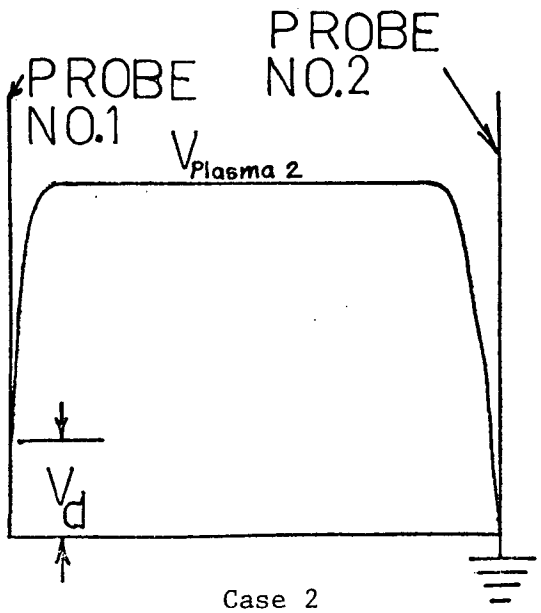

Case 2

Fig. 2b

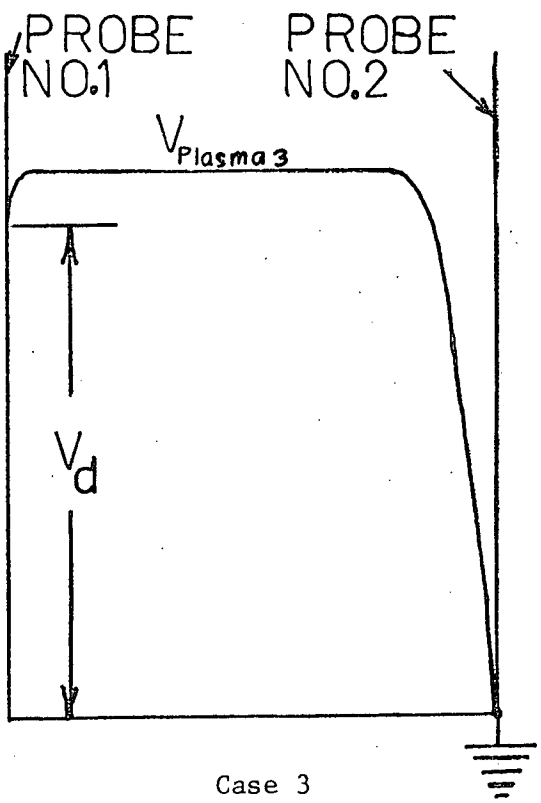

Case 3

Fig. 2c

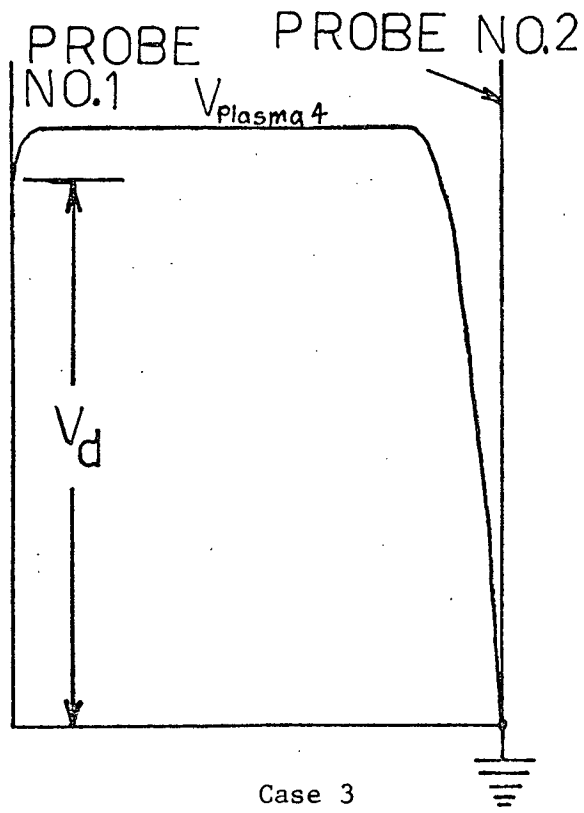

Case 3

Fig. 2d

from the plasma. Thus half of the electrons arriving at probe (1) pass through the external circuit to make up for the deficiency of electrons at probe (2). Any further positive increase in the value of V_d will not cause any further increase in the current through the external circuit because probe (1) is already drawing enough electrons from the plasma to balance all the ion current flowing in the system. The further increases in V_d will only raise the plasma potential higher, but will not change the potential difference between the plasma potential and probe (1). Probe (2) thus becomes more negative with respect to the plasma potential and is thus saturated with respect to positive ions. The potential diagram for case 3 is shown in Figures 2c and 2d.

Case 4 occurs when V_d is slightly negative so that probe (1) draws less electrons than probe (2). With fewer electrons leaving the plasma than ions the plasma potential drops so that more electrons reach probe (2) and the excess of electrons which arrive at probe (2) pass through the external circuit to compensate for the deficiency of electrons at probe (1). The potential diagram for case 4 is shown in Figure 2e.

Case 5 occurs when V_d is made strongly negative such that probe (1) does not draw any electrons from the plasma causing the plasma potential to fall as more positive ions are leaving the plasma than are electrons. Due to the fall in the plasma potential probe (2) draws more electrons, half of which flow through the external circuit to compensate for the deficiency of electrons at probe (1). If V_d is made more strongly negative the potential difference between the plasma and probe (2) will not change, as probe (2) is already drawing enough electrons from the plasma to balance all the ion current flowing in the system. Thus by

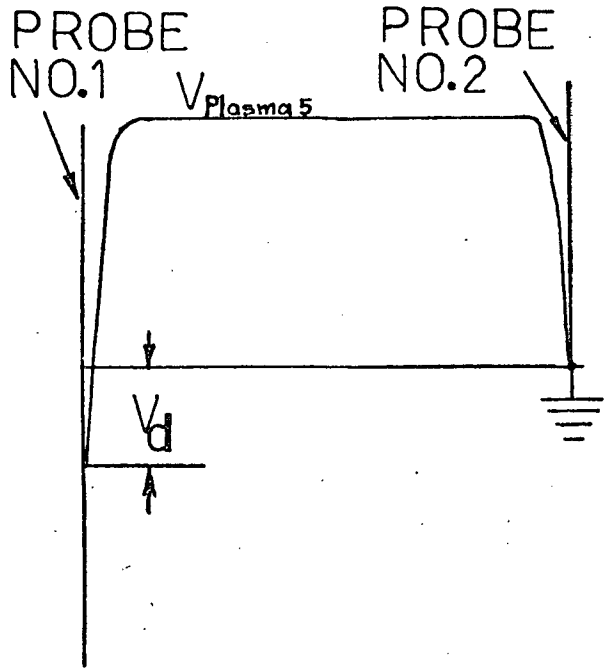

Case 4

Fig. 2e

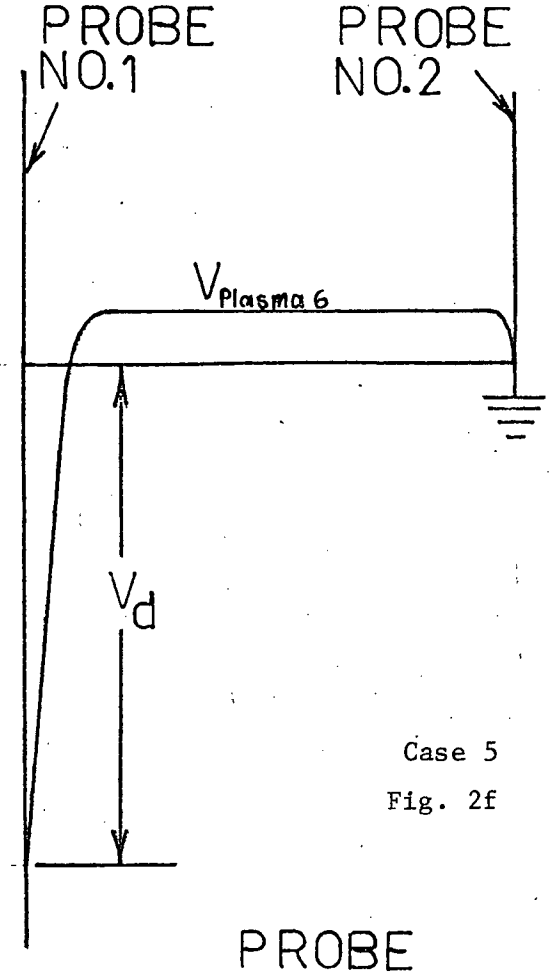

Case 5

Fig. 2f

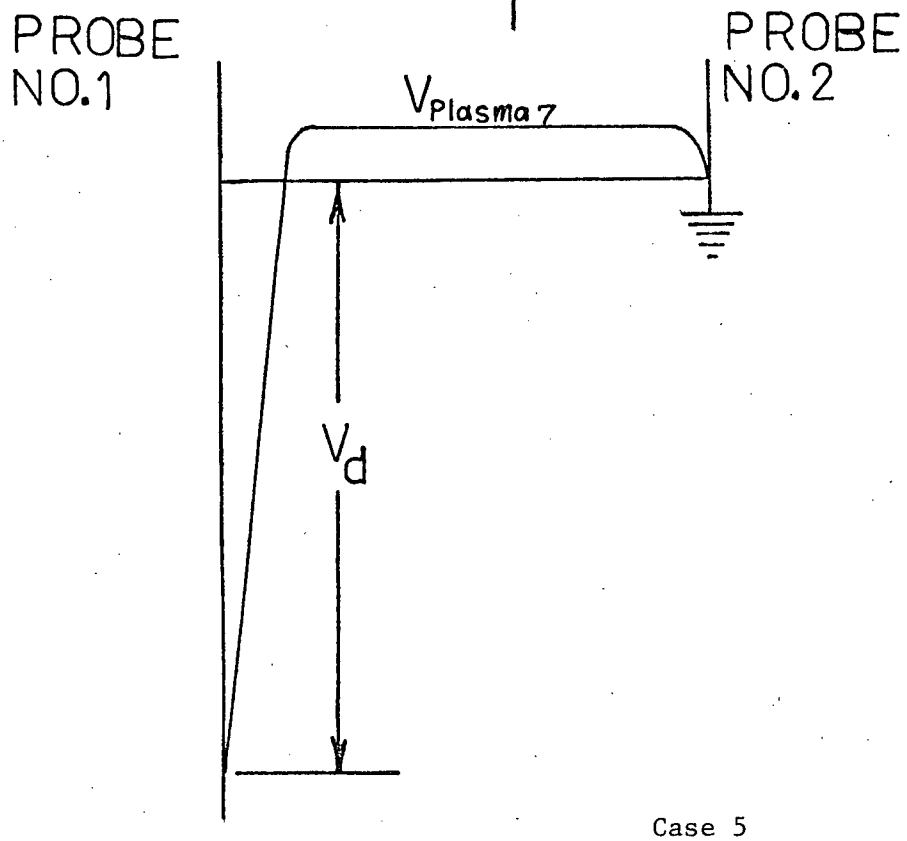

Case 5

Fig. 2g

V_d going further negative the potential of probe (1) will become further negative with respect to the plasma potential, but the plasma potential will not change. The potential diagram for case 5 is shown in Figures 2f and 2g.

Figure 3 shows the curve of I_d vs. V_d for the cases discussed above. For the experiment explained in this thesis the part of Figure 3 where V_d is negative was not needed. When the probe areas are not equal and or $V_c \neq 0$ the curve will not cross the V_d axis where $V_d = 0$, but it will still have the same form.

Figure 4 shows the potential diagram, for two different film thicknesses, when a constant voltage, V_{supply}, is applied to the sample.

In Figure 4 a constant voltage was applied when the film thickness was D_1 and the oxide drew an initial current I_1. The film was allowed to grow to a thickness D_2 where it drew a final current I_2. By replacing the oxide film by a metal electrode of the same area as the film surface area a curve can be obtained as in Figure 3. The values of V_{d1} and V_{d2} can then be obtained from Figure 3 by finding the voltages corresponding to I_1 and I_2.

Since electrode number 2 is grounded and at zero voltage, the initial voltage across the oxide film, when the film thickness is D_1, is U_1 and the final voltage across the oxide film is U_2, when the film thickness is D_2, where U_1 and U_2 are given by (1) and (2) respectively.

$$U_1 = V_{supply} - V_{d1} \qquad (1)$$

$$U_2 = V_{supply} - V_{d2} \qquad (2)$$

The change in voltage across the oxide film in growing from its initial to final thickness is defined by ΔU which is given by (3).

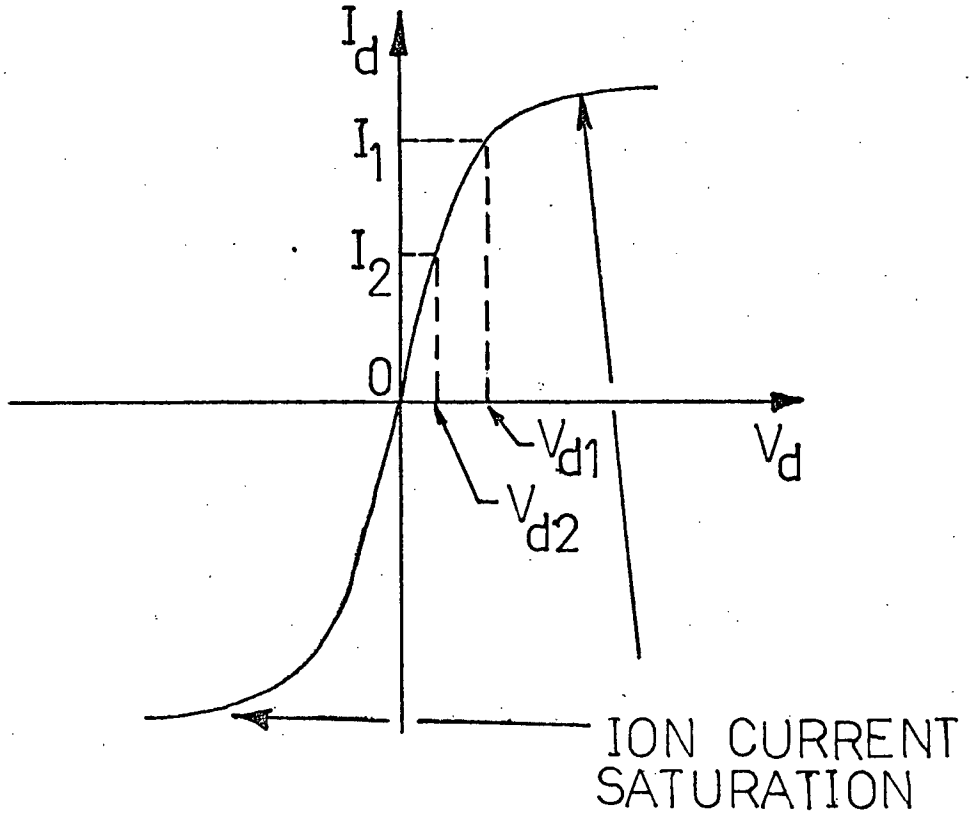
I_d
I_1
I_2
0
V_{d1}
V_{d2}
V_d
ION CURRENT SATURATION

Fig. (3)

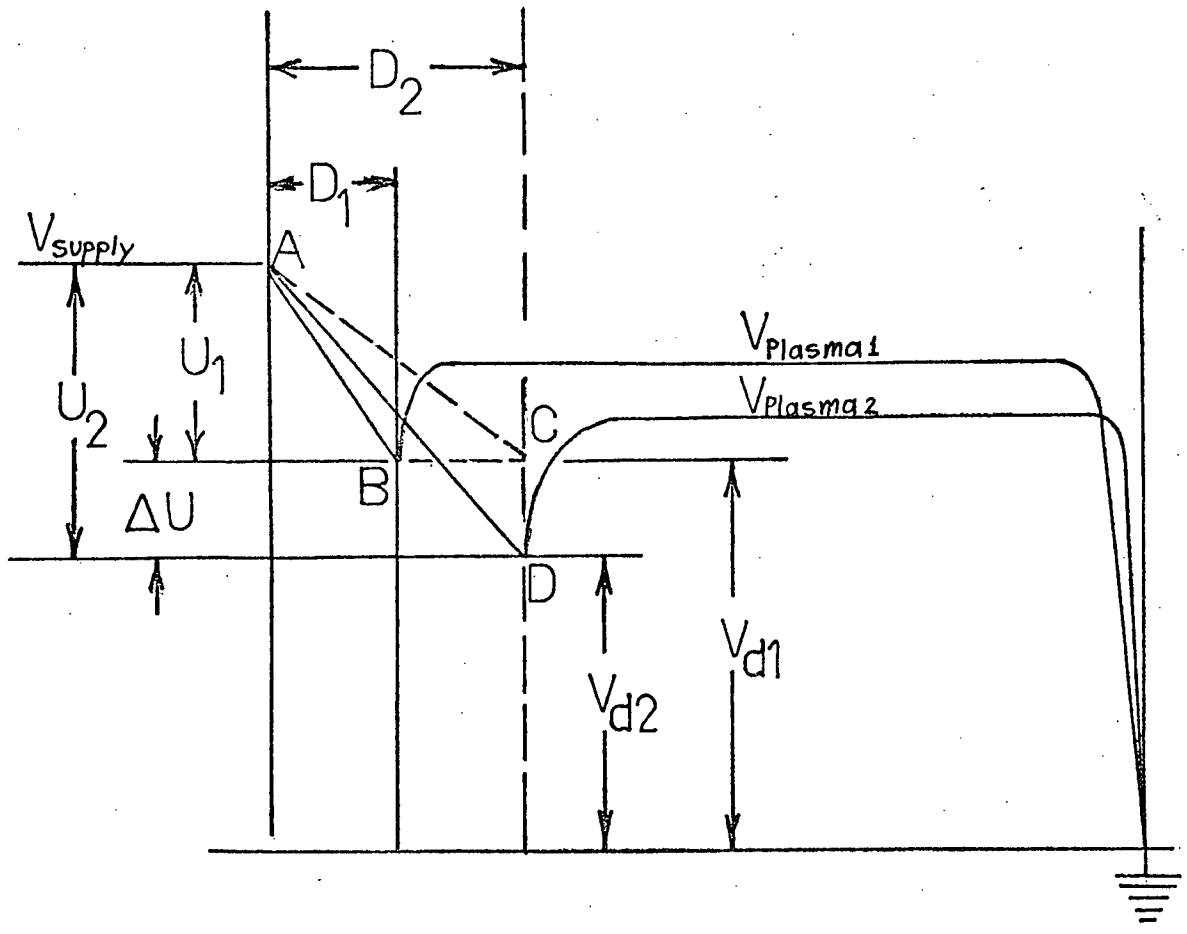
D_2
D_1
V_{supply}
A
U_1
U_2
ΔU
B
C
D
$V_{Plasma1}$
$V_{Plasma2}$
V_{d1}
V_{d2}

Fig. (4)

$$\Delta U \equiv U_2 - U_1 = V_{d1} - V_{d2} \tag{3}$$

The voltage regulation during the film growth from D_1 to D_2 is given by (4).

$$(\text{percent voltage regulation}) \equiv \frac{\Delta U}{U_1} \times 100 = \frac{V_{d1} - V_{d2}}{V_{supply} - V_{d1}} \times 100 \tag{4}$$

If $V_{supply} >> V_{d1}$ and if the difference between V_{d1} and V_{d2} is small compared to V_{supply} the voltage regulation will be quite small. The condition that $V_{supply} >> V_{d1}$ can be obtained by having a film of good insulating quality and the condition that $V_{d1} - V_{d2} << V_{supply}$ can be obtained by not operating in the saturation region of Figure (3).

It is useful to consider also the electric field in the oxide film. The initial field in the oxide film is the slope of the line AB in Figure (4) which is given by (5).

$$E_1 = \frac{U_1}{D_1} \tag{5}$$

The actual final field in the oxide film is $(E_2)_{actual}$ and is the slope of the line AD in Figure (4) which is given by (6).

$$(E_2)_{actual} = \frac{U_2}{D_2} \tag{6}$$

It is of interest to define the field that would be in the oxide film if V_{d1} did not change with film thickness so that the field change in the oxide was only due to the change in the thickness of the film and not also to a change in voltage across the oxide film. This field is defined as $(E_2)_{theoretical}$ and is the slope of line AC in Figure (4) which is given by (7).

$$(E_2)_{theoretical} = \frac{U_1}{D_2} \tag{7}$$

The theoretical field change due only to the change in thickness of the film is denoted by $(\Delta E)_{theoretical}$ and is given by (8).

$$(\Delta E)_{theoretical} = E_1 - (E_2)_{theoretical} = U_1(\frac{1}{D_1} - \frac{1}{D_2}) \qquad (8)$$

The actual field change due to the combination of a film thickness change and the change in the potential across the film is denoted by $(\Delta E)_{actual}$ and is given by (9).

$$(\Delta E)_{actual} = E_1 - (E_2)_{actual} = \frac{U_1}{D_1} - \frac{U_2}{D_2} \qquad (9)$$

The percent error between the theoretical field change and the actual field change, denoted by the Greek letter γ, is given by (10).

$$\gamma = \frac{(\Delta E)_{theoretical} - (\Delta E)_{actual}}{E_1} \times 100 = \frac{D_1}{D_2}\frac{U_2 - U_1}{U_1} \times 100 = \frac{D_1}{D_2}\{\text{percent voltage regulation}\} \qquad (10)$$

The value of γ is a measure of whether the voltage regulation took place over a small or large interval of film thickness. For a fixed voltage regulation γ will be larger if the regulation took place over a small interval of film thickness than over a large interval of film thickness.

REFERENCES

1. C.J. Dell'Oca, D. Pulfrey and L. Young, Physics of Thin Films, 6 (in press).
2. J.F. O'Hanlon, J. Vac. Sci. and Tech., 7, 330 (1970).
3. R. I. Nazarova, Russ J. Phys. Chem., 36, 522 (1962).
4. J. R. Ligenza, J. Appl. Phys., 36, 2703 (1965).
5. J. Kraitchman, J. Appl. Phys., 38, 4323 (1967).
6. P.J. Jorgensen, J. Chem. Phys., 37, 874 (1962).
7. W.L. Lee, G. Olive, D.L. Pulfrey, and L. Young, J. Electrochem. Soc., 11, 1172, (1970).
8. B.E. Deal and A.S. Grove, J. Appl. Phys., 36, 3770 (1965).
9. L. Young, Anodic Oxide Films, Academic press: London (1961).
10. L. Young and F.G.R. Zobel, Electrochm. Soc., 113, 277 (1966).
11. C.R. Fritzshe, Solid State Comm., 6, 341 (1968).
12. C.R. Fritzsche, J. Phys. Chem. Solids, 30, 1885 (1969).
13. S. Whitehead, Dielectric Breakdown of Solids, Oxford: London (1951).
14. O.S. Heavens, Optical Properties of Thin Solid Films, Butterworths: London (1955).
15. I. Franz and W. Langheinrich, Sol. Stat. Electr., 11, 63, (1968).
16. T.E. French and C.J. Vierck, Graphic Science, McGraw-Hill, 1st. ed., 676, (1958).
17. R.M. Burger and R.P. Donovan, Fundamentals of Silicon Integrated Device Technology, Prentice Hall: New York, 5 (1967).
18. C.R. Fritzshe, Z. Angew. Phys., 24, 48 (1967).
19. A.M. Goodman, J. Electrochem. Soc., 115, 281, (1968).
20. E.O. Johnson and L. Malter, Phys. Rev., 80, 58, (1950).

21. L. Masing, J.E. Orme, and L. Young, J. Electrochem. Soc., 108, 428, (1961).

22. M.J. Rand, J. Appl. Phys., 41, 787 (1970).